Components-bandgap relationships in hybrid organic-inorganic perovskites

Shanti Maria Liga

February 2017

Literature Thesis (12 ECTS)

Under supervision of:

Dr. Sarah Brittman

Dr. Elizabeth von Hauff

UNIVERSITEIT VAN AMSTERDAM

Abstract

Over the last 8 years, hybrid organic-inorganic perovskite solar cells have shown a tremendous increase in power conversion efficiencies, reaching 22.1% in 2016. A remarkable feature of this material is the possibility of controlling its properties by chemical management, namely by changing its elemental composition. One key parameter for solar cells is the optical bandgap, which strongly depends on the elemental composition of the perovskite. The role played by each component in generating the bandgap is still under debate, but it has already been demonstrated through simulations and experimental evidence that it correlates with simple structural features, such as the X-B-X angles and the B-X distance in the octahedral framework, the size of the organic cation and its interactions with the inorganic components. Taking into account these correlations helps in improving the light harvesting efficiency of this material, which can assume a bandgap between 1.1 eV and 3.1 eV depending on the elements of which it is composed. This tunability offers the possibility of fabricating colourful solar cells and suitable materials for tandem solar cells.

Contents

Abstract **2**

Introduction **5**

Chapter 1. Crystal structures and electronic structure **6**

Chapter 2. The inorganic anion **10**

2.1 Influence of the electronegativity of the X anion 10

2.2 Influence of the lattice constant 11

2.3 Current state of the art 12

2.3.1 $MAPbX_3$ halide perovskites, pure and mixed forms 12

2.3.2 $MAPbX_3$, polyanions perovskites 15

2.3.3 $FAPbX_3$, formamidinium halide perovskites 15

2.4 Discussion 15

Chapter 3. The inorganic cation **17**

3.1 Current state of the art 17

3.1.1 One B component perovskites 17

3.1.2 Mixed Pb-Sn perovskites 18

3.1.3 Doped $CH_3NH_3PbI_3$ perovskites in Pb^{2+} sites 19

3.1.4 Lead- Free forms 20

3.2 Discussion 21

Chapter 4. The organic cation **22**

4.1 Influence on X-B-X angles 22

4.2 Influence through H bonding 24

4.3 Current state of the art 25

4.3.1 Perovskites with one A component 25

4.3.2 Mixed organic perovskites 27

4.3.3 Mixed organic-inorganic perovskites 28

4.3.4 A study on $CsPbI_3$ 30

Discussion **30**

References **32**

Appendix **37**

Introduction.

Hybrid organic-inorganic perovskites recently triggered tremendous research interest following the astonishing progress of the efficiency of their solar cells, which in less than 8 years of intense research have reached an efficiency of 22.1% (NREL). This impressive trend has revolutionized solar cell research and encouraged many research groups to focus on these appealing solution-processable semiconductors.

Perovskites are, in general, any materials with the same cubic crystal structure of calcium titanate and chemical formula ABX_3[1]. Those used in solar cells are called hybrid organic-inorganic perovskites because they are composed of a big organic cation, A, and an inorganic framework, constituted by a metallic cation B, and an anion, X. The most common used organic cation is methylammonium ($CH_3NH_3^+$), while the X component is usually a halide, Cl^-, Br^- or I^- and B is most frequently lead.

Organic-inorganic iodoplumbate and bromostannate perovskites were synthesised for the first time in 1978[2,3]. Around 15 years later, the studies of Mitzi et al.[4,5] highlighted the semiconducting properties of perovskites. However, they were employed in photovoltaic application only in 2009, when for the first time methylammonium lead iodide ($MAPbI_3$) was used in a liquid-electrolyte-based dye-sensitized solar cells, reaching an efficiency of 3.9%[6]. In addition to its impressive performance as light harvester, $MAPbI_3$ shown also its main drawback, namely its instability in the electrolyte. Therefore, in the next years, the electrolyte was replaced with a solid organic hole conductor[7,8,9]. While investigating the charge-transport properties of a perovskite deposited on mesoporous Al_2O_3, it was for the first time recognized that methylammonium halide plumbates were not only good light harvesters but could also act as n-type component in dye-sensitised solar cells, transporting the electrons through their thickness to the electrode surface[10]. In the meanwhile, other studies shown that it could also perform as p-type layer[7,11]. These discoveries triggered the research to evolve towards perovskite thin film solar cells.

Perovskites have drawn great interest because they show a combination of organic and inorganic characteristics that make them unique materials. Indeed, the long charge carrier lifetime[12] and diffusion length[13] in combination with the high absorption coefficient[14] and their synthesis, which involves low-temperature and solution-based deposition, are all features that usually do not appear in the same material. However, they still show two fundamental problems that the research community has not yet solved. The first one is instability, which hampers the commercialization of perovskite solar cells. The second one is the presence of lead in the structure, since it is a toxic element and its release in the environment is a considerable concern.

Even though perovskites have been the subject of intense and successful research over the last few years, the understanding of their properties is still under debate. Finding the relationship between the chemical structure and the resulting properties is a useful tool to overcome some fundamental issues that limit further development. Moreover, understanding the mechanisms behind the empirical results helps to rationalize future research.

Since one of their roles in a solar cell is light harvesting, the correlation between the bandgap and the components has been the subject of a lot of research. Some correlations between the bandgap width, the properties of the components and their interactions have been highlighted. The optimization of the bandgap to make solar cells with efficiencies close to that imposed by the Shockley-Queisser limit

is not the only objective of this research. Indeed, a motivation to fabricate lower bandgap perovskites is that of use them for the bottom of tandem solar cells.

In the next pages, an overview of the scientific work that focuses on this topic is given. The role played by each ion in tuning the optical bandgap is discussed based on theoretical and experimental studies. The literature study shows also some discrepancies in the bandgap values measured by different studies and some explanations are provided to account for these differences at the end of each chapter and in the Appendix.

Chapter 1. Crystal structures and electronic structure

Hybrid organic-inorganic halide perovskites belong to the wide family of metal-organic frameworks (MOFs), which have drawn great interest over the last few decades because of their special properties suitable for optoelectronic applications. The general chemical formula of perovskites is ABX_3, in which A and B are cations, the former larger than the latter, and X is the anion.

The inorganic cation and the halide form an octahedral inorganic framework with a ReO_3-structure type[15], while the organic cation A is located in the vacancies between the octahedra and at room temperature is freely rotating[16]. Figure 1 shows the archetypical cubic structure.

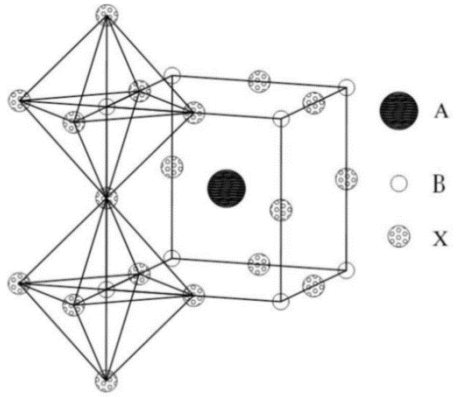

Figure 1: Cubic perovskite structure of ABX_3

Depending on the size and nature of the components[17], on the interactions between them[18] and on the temperature, this ideal structure distorts to tetragonal and orthorhombic structures. In the most common perovskites used in photovoltaic applications, A is methylammonium (MA^+), B is lead (Pb^{2+}) and X is a halide. All the methylammonium lead halide perovskites $MAPbX_3$ show the same trend, presenting a cubic phase at high temperature, a tetragonal phase at intermediate temperature and an orthorhombic phase at low temperature[19]. However, every perovskite has its specific transition temperatures so that, for instance, at room temperature $MAPbI_3$ has a tetragonal structure, while $MAPbBr_3$ and $MAPbCl_3$ have a cubic one[18]. In table 1, an overview of the phase transition temperatures for the three most common halide perovskites is given.

Material	$CH_3NH_3PbCl_3$	$CH_3NH_3PbBr_3$	$CH_3NH_3PbI_3$
Crystal system	Cubic	Cubic	Cubic
Transition temperature (K)	177	236	330
Crystal system	Tetragonal	Tetragonal	Tetragonal
Transition temperature (K)	172	149~154	161
Crystal system	Orthorhombic	Orthorhombic	Orthorhombic

Table 1: Crystal system and transition temperature (K) for the most common halide perovskites[20].

At high temperature, all ions that compose the cubic structure are freely rotating in every direction. Lowering the temperature, the halide ions get ordered, namely they start having

preferred positions, so that the symmetry of the system shifts from cubic to tetragonal. The further decrease in temperature causes the ordering of MA ions, which determines the transformation from the tetragonal phase to the even less symmetric orthorhombic one. Figure 2 depicts the three structure phases and show the preferred directions to which the different components direct upon cooling.

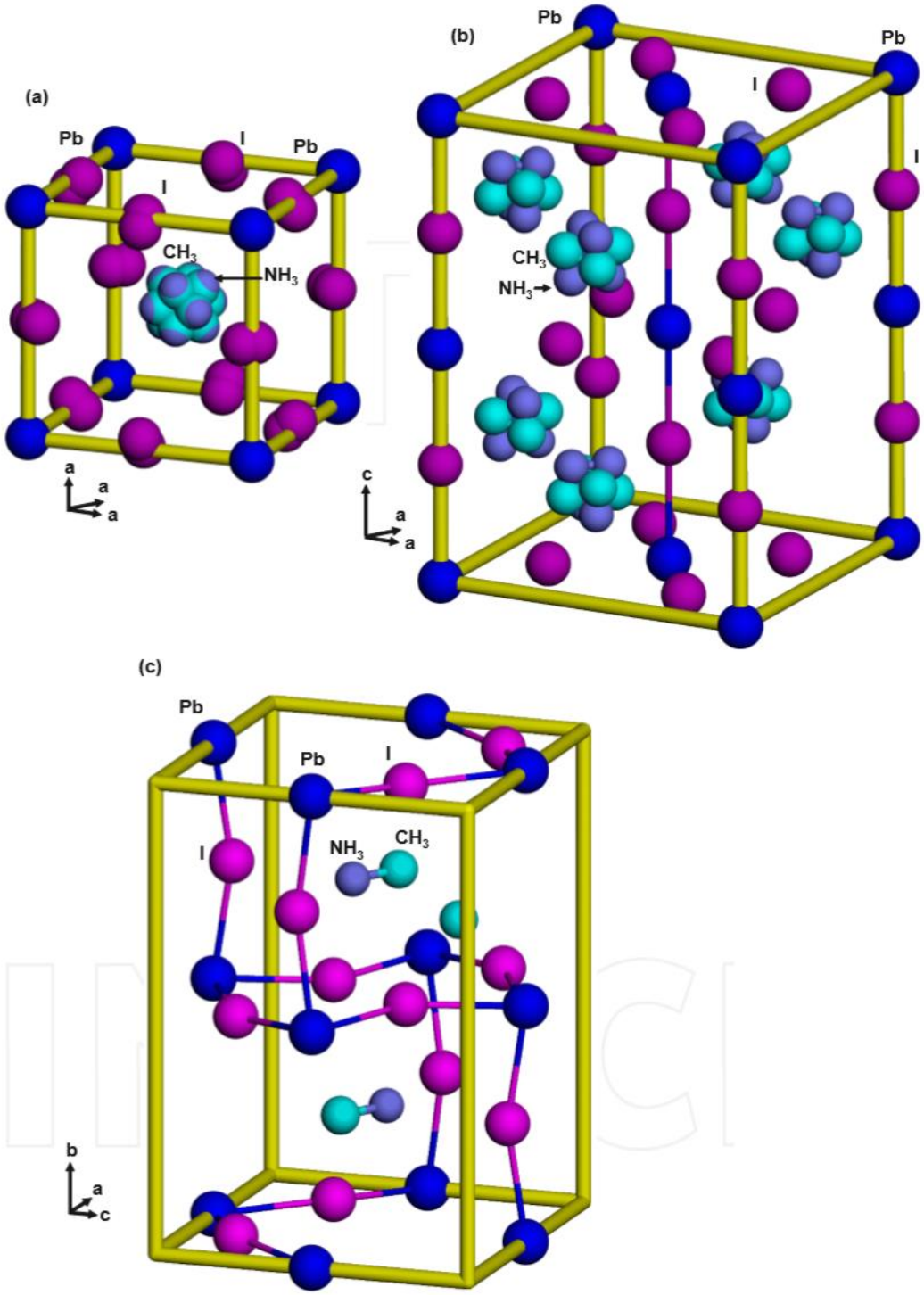

Figure 2: Structure models of the cubic (a), tetragonal (b) and orthorhombic (c) phases of methylammonium lead iodide[20].

The discrepancy in transition temperatures for the three halide perovskites stems from the different type of interactions between the components of the crystal[18]. Four different interactions can be considered in order to classify the type of chemical bonds within the lattice[16]:

- Electrostatic interactions, which occur between the inorganic components and between the positive charged organic cation and the negative charged inorganic framework, with lead having a formal oxidation state of +2, the halide of -1 and the organic cation of +1.
- Dipole-dipole interactions between organic cations close to each other.
- Charge-dipole interactions between the inorganic octahedron and the organic counterpart.
- Induced dipole interactions, also called Debye interactions, between the halide and the acidic hydrogen present in the organic cation. This interaction is stronger when the halide is more polarizable, so it increases going down in the periodic table, and depending on the acidity of the proton in the organic ion. For instance, as said before, taking into consideration the methylammonium perovskites, at room temperature the iodide perovskite is already deformed while the bromide and the chloride ones are not. This suggests that the interactions between the halide and the proton are stronger for the iodide than for the other halides, and this is indeed the case because the iodide is the biggest halide and therefore the most polarizable. In most of the works[19,21,22], this interaction has been described as a hydrogen bonding, while other studies[16] prefer to use the more general definition of induced dipole interaction because, since at room temperature the organic ion is freely rotating, a defined bonding is difficult to imagine.

  These four interactions contribute to the deformation of the archetypical cubic structure, so that their consideration is fundamental in order to understand how the perovskite's properties change depending on the nature of the ions of which it is composed.

Over the last few years, many combinations of organic molecules and inorganic ions have been tested to prepare perovskites with high conductivity and bandgap close to the optimal for reaching the Shockley-Queisser limit[23], namely around 1.4 eV. The formability of perovskites, namely the possibility that the combination of 2 cations and one anion gives rise to the perovskite structure, has been the subject of many studies[24,25,26] that were aimed at finding any parameters through which the formation could be predicted. Some of these studies focused on the formation of perovskites with formula ABO_3, while others investigate the formation of halide perovskites.
Good accuracy is obtained when the formation of perovskites is predicted by considering two parameters, namely the Goldschmidt tolerance factor and the octahedral factor[24]. Both the parameters have a physical meaning and each one has been found to be a necessary but not sufficient condition for the formation of the perovskite[15].
The Goldschmidt tolerance factor, α, is a geometrical parameter defined as

$$\alpha = \frac{(r_A + r_x)}{\sqrt{2}(r_B + r_x)}$$

where r_i is the radius of ions in the perovskite ABX_3. The ionic radius of the molecular organic cation depends on its anionic counterpart, because it varies depending on the nature of the hydrogen interactions. However, by applying a rigid sphere model, the effective radii of many organic cations have already been calculated from crystallographic data[27], so that a rough estimation of α is possible. The optimal α value for cubic perovskite structures has been set between 0.9 and 1[28]. However, as suggested above, this parameter is a necessary but not sufficient condition for the formation of the perovskite. This means that compounds with a tolerance factor

between 0.9 and 1 might not be perovskites if their octahedral factor does not fall in the suitable range.
The octahedral factor concerns only the inorganic framework of the structure. Indeed, it is equal to the ratio

$$\mu = r_B/r_X$$

and the optimal values for forming a perovskite have been found to be between 0.414 and 0.732[15]. The optimal values of α and μ have been determined by drawing a α-μ structure map of more than 150 ABX_3 compounds.

In addition to the crystal structure overview, a glimpse of the electronic structure helps in further comprehending the properties of perovskites. As shown in figure 3 for the lead case, the valance band is generated by the overlap of Pb 6s orbitals and X np orbitals, where n depends on the nature of the X. This combination gives rise to the anti-bonding orbital of the inorganic framework. The conduction band is formed of the antibonding combination of empty Pb 6p orbitals, that with a formal oxidation state of 2+ has the electronic configuration 5d10 6s2 6p0[29], and only in small portion by the X ns orbitals. This implies that the organic cation does not play a significant role in the formation of the frontier orbitals[29]. However, as discussed in chapter 4, the organic molecule influences indirectly the bandgap of the material, which is not surprising since, as discussed above, it interacts in more than one way with the inorganic counterpart.

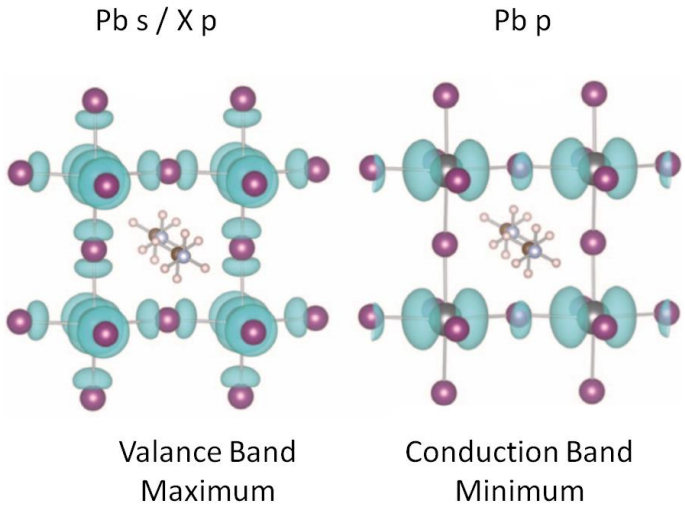

Figure 3: Frontier orbitals of methylammonium halide perovskites[29]

Chapter 2. The inorganic anion

Influence of the electronegativity of the X anion.

As mentioned in Chapter 1, the valance band is the result of the antibonding combination of Pb 6s orbitals and X np orbitals, while the conduction band is mainly formed by empty Pb 6p orbitals.

A computational study on $CsSnX_3$ perovskites[30] found a clear correlation between both the electronegativity of the halide ion and the bandgap, and the lattice constant of the crystal and the bandgap. Making use of quasiparticle self-consistent GW (QSGW) electronic structure calculations, the results fit the experimental values. Figure 4 shows the band structures and partial densities of states of the cubic phases of the three $CsPbX_3$, where X is I^-, Br^- or Cl^- .

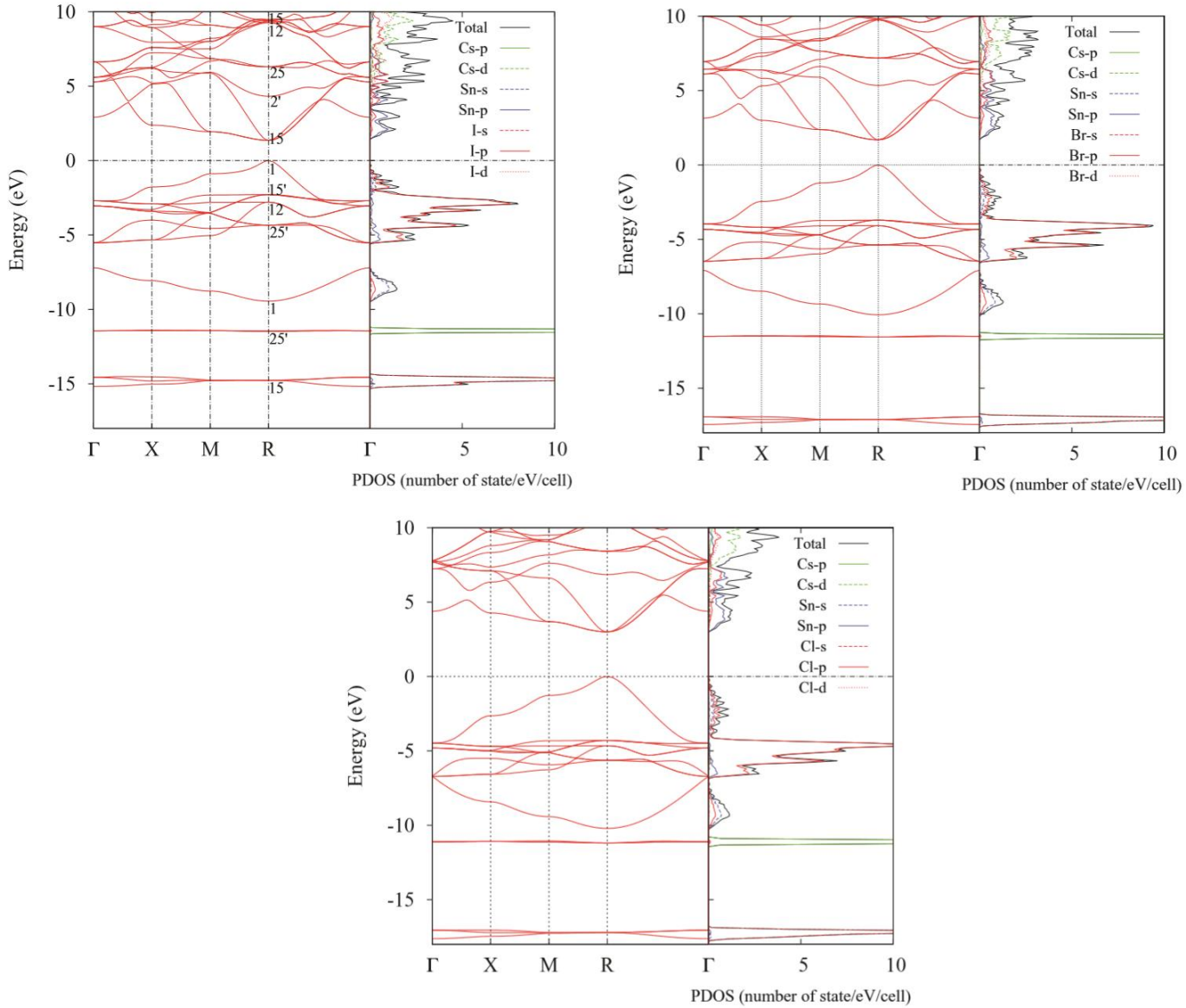

Figure 4: Band structures and partial densities of states of cubic $CsSnI_3$, $CsSnBr_3$ and $CsSnCl_3$[30].

The analysis of the orbital character of the bands is a good starting point to determine how the halide influences the change in the bandgap value. Looking at the $CsSnI_3$ band structure, the lowest bands are the I 5s bands. Of course, by increasing the electronegativity of the halide, these bands move

farther down in the energy axis. The second band starting from below is that of the Cs 5p, followed by the band corresponding to the bonding combination of Sn 5s and I 5p orbitals. The next series of bands are generated by I 5p states, while the band corresponding to the valance band maximum (VBM) is produced by the antibonding combination of Sn 5s and I 5p orbitals. The conduction band minimum (CBM) has mostly a Sn 5 p character, while above there are still I 5p and then Cs 5d contributions. The minimum value of the bandgap is at the R point.

The analysis of the band structure clarifies the reasons why perovskites with more electronegative halides have broader bandgap. Indeed, as the electronegativity raises, the X np orbitals (where n is 5 for I^-, 4 for Br^- and 3 for Cl^-) are held more tightly by the nucleus and therefore have a lower energy. This causes a worse interaction with the Sn 5s orbitals. Therefore, as the interaction between the orbitals of the two elements diminishes due to a higher energy gap, the bonding orbital will be less stabilized by this interaction and the antibonding orbital less destabilized. Thus, the latter will assume a lower energy as compared to the case of strong interaction (Figure 5). The VBM energy drop implies, of course, an increase in bandgap.

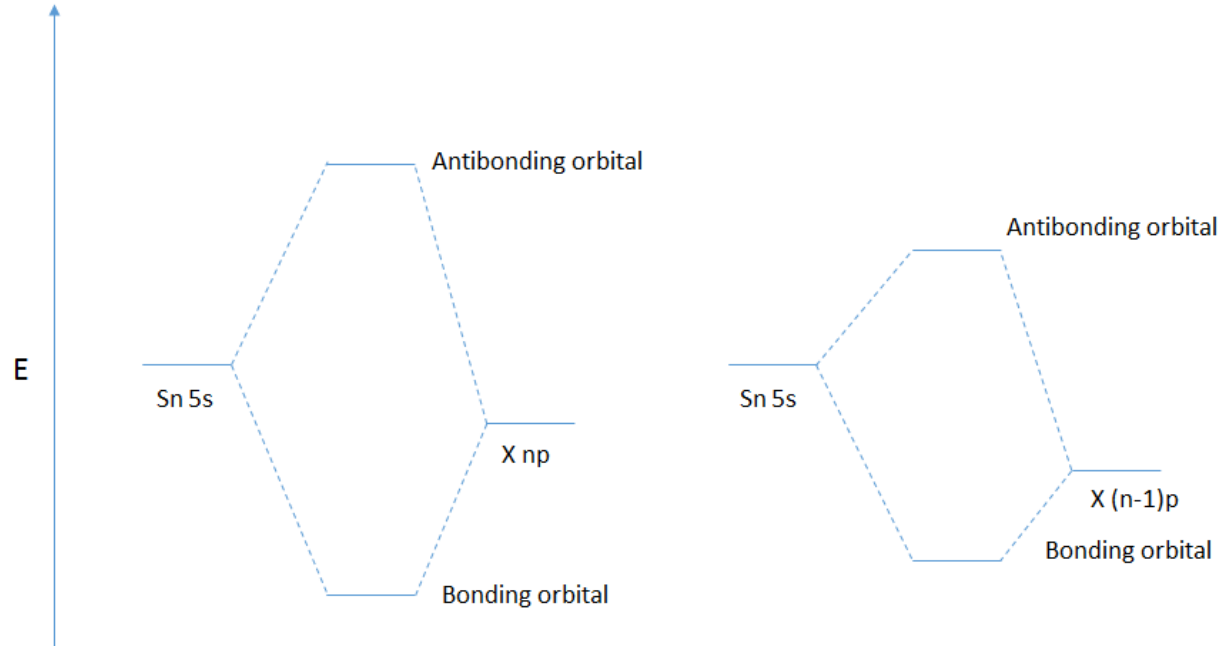

Figure 5: Qualitative representation of the bonding and antibonding interaction for 2 X with different atomic orbitals energy.

Influence of the lattice constant.

In addition to the electronegativity-bandgap correlation, when considering the same perovskite but in different crystal phases, a relationship between the lattice constant and the bandgap exists[30]. Indeed, when the lattice constant is bigger, the B and X ions are further apart and the orbitals in opposite phases repel with lower energy, so that also in this case, the valance band has a lower energy and the bandgap broadens. Figure 6 depicts the p orbitals of X pointing towards the Sn 5s orbital at the centre of the unit cell. When the lattice parameter is bigger, both the bonding and the antibonding interactions between the orbitals of B and X are reduced.

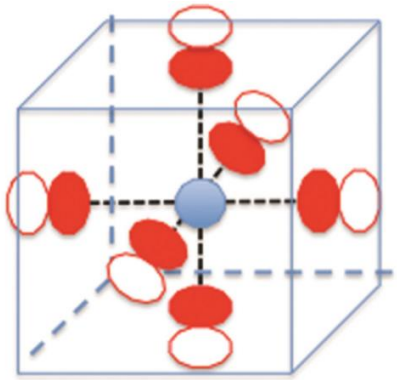

Figure 6: Representation of the X p orbitals pointing towards the Sn 5s orbital at the centre of the unit cell[30]

Current state of the art.

MAPbX$_3$ halide perovskites, pure and mixed forms.

As discussed in the first chapter, as the temperature drops, the crystal structure of the perovskite distorts and passes from cubic to tetragonal to orthorhombic. This change in symmetry influences also the value of the lattice parameters, which, as previously shown, have a direct impact on the value of the bandgap. It has been calculated through simulations for the case of $MAPbI_3$[31] that by shifting from the cubic structure to the tetragonal and from the latter to the orthorhombic the lattice parameters grow progressively and the bandgap rises from 1.3 eV, to 1.43 eV to 1.61 eV. The bandgap at room temperature, when this perovskite assumes a tetragonal structure, has been calculated experimentally to be 1.51 eV. This value was extrapolated from diffuse reflectance UV-Vis spectra using the Kubelka-Munk equation to convert it to absorption spectra and it is slightly higher that the calculated one due to underestimation with the DFT using GGA calculation.

At a given temperature, the bandgap of $MAPbI_3$ can be easily tuned by replacing the iodide with another anion. As calculated from computational studies, when I^- is replaced by a more electronegative anion of the VII group of the periodic table, the bandgap broadens. This phenomenon was demonstrated experimentally many times and by using different methods[32,33,34]. One of the latest work measured not only the bandgap but also the valance and conduction bands energies. The first one extrapolated from Tauc plots with data taken from UV-vis absorption measurements and the second ones through direct and inverse photoemission studies[32]. Not only the electronic properties of pure MAPbX$_3$ perovskites were investigated, but also those of mixed halide species, namely $MAPbI_{2.1}Br_{0.9}$, $MAPbBr_{1.5}Br_{1.5}$ and $MAPbI_{2.1}Cl_{0.9}$. However, from the XRD spectra it is not very clear if the ratio of the two halides is actually the one indicated in the formula, which refers to the ratios of precursors used. Other previous studies[35] indicated the impossibility to form a one phase film of $MAPbI_{3-x}Cl_x$ with a percentage of Cl higher than 4%. Figure 7 shows the results obtained from direct and inverse photoemission measurements while in the table the results for the optical bandgap and the calculated exciton binding energy are given.

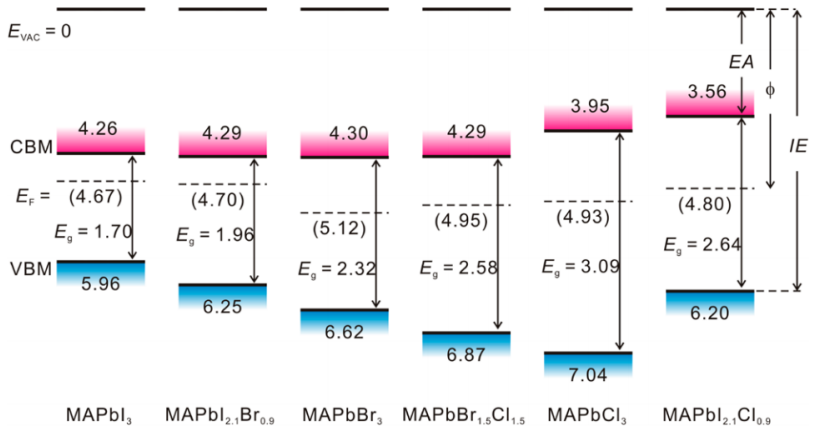

Table 1. Comparisons of Charge Transport Band Gap (E_g) and Optical Band Gap (E_{opt})

materials	E_g (eV)	E_{opt} (eV)	Δ (eV)
$MAPbI_3$	1.70 ± 0.10	1.52 ± 0.02	0.18 ± 0.10
$MAPbBr_3$	2.32 ± 0.10	1.84 ± 0.04	0.48 ± 0.11
$MAPbCl_3$	3.09 ± 0.10	2.97 ± 0.07	0.12 ± 0.12
$MAPbI_{2.1}Br_{0.9}$	1.96 ± 0.10	1.80 ± 0.02	0.16 ± 0.10
$MAPbI_{2.1}Cl_{0.9}$	2.64 ± 0.10	2.60 ± 0.05	0.04 ± 0.11
$MAPbBr_{1.5}Cl_{1.5}$	2.58 ± 0.10	2.44 ± 0.10	0.14 ± 0.14

[a]The exciton binding energy (Δ) is obtained by the difference between E_g and E_{opt}. The experimental errors of E_{opt} were determined by the average of five samples.

Figure 7: Energy level diagrams of various perovskite films experimentally derived from ultraviolet direct and inverse photoemission spectra with a common vacuum level. The numbers in parentheses give the work functions. The table shows the E_g, E_{opt} and the difference between these two with an error calculated by measuring 5 samples[32].

The results shown in the table are in line with the theoretical explanation given in the previous section. As the electronegativity of X increases, the interaction between Pb and X drops and the bandgap increases, so that $E_g(MAPbI_3) < E_g(MAPbBr_3) < E_g(MAPbCl_3)$. Moreover, the bandgap of all the mixed forms has a value between that of the two pure forms.

The closest elementary anion to iodide with regard to the electronic properties and the size is the bromide. It was demonstrated that the entire range of alloys with formula $MAPb(I_{1-x}Br_x)_3$ can be synthesised from solution and that these alloys do not show phase segregation[33]in the dark[36]. The variation of the bandgap in the alloyed hybrid perovskites was measured from the onset of the UV-visible absorption spectra of the perovskite deposited on mesoporous TiO_2, as shown in figure 8a. By increasing the bromide ratio, the bandgap is tuned from 1.58 eV to 2.28 eV when x= 1. This bandgap shift allows the fabrication of colourful devices as shown in figure 8b.

In order to see how miscible is the $MAPbI_3/MAPbBr_3$ alloy, the Vegard's law can be applied. In general, it correlates the molar fraction of the components with the change in properties of the alloy. Figure 8c depicts the value of the bandgap as a function of the Br composition. Empirically, the nonlinear variation of the bandgap with the Br ratio, which could be caused by the anisotropic nature of binding, can be expressed as:

$$E_g[MAPb(_{I1-x}Br_x)_3] = Eg[MAPbI_3] + (Eg[MAPbBr_3] - Eg[MAPbI_3] - b)x + bx^2$$

where b is the bowing parameter. For this case, b has been calculated to be 0.33, which is a value small enough to consider a good miscibility of the two perovskites. The miscibility is determined by the small difference in size and properties of iodide and bromide.

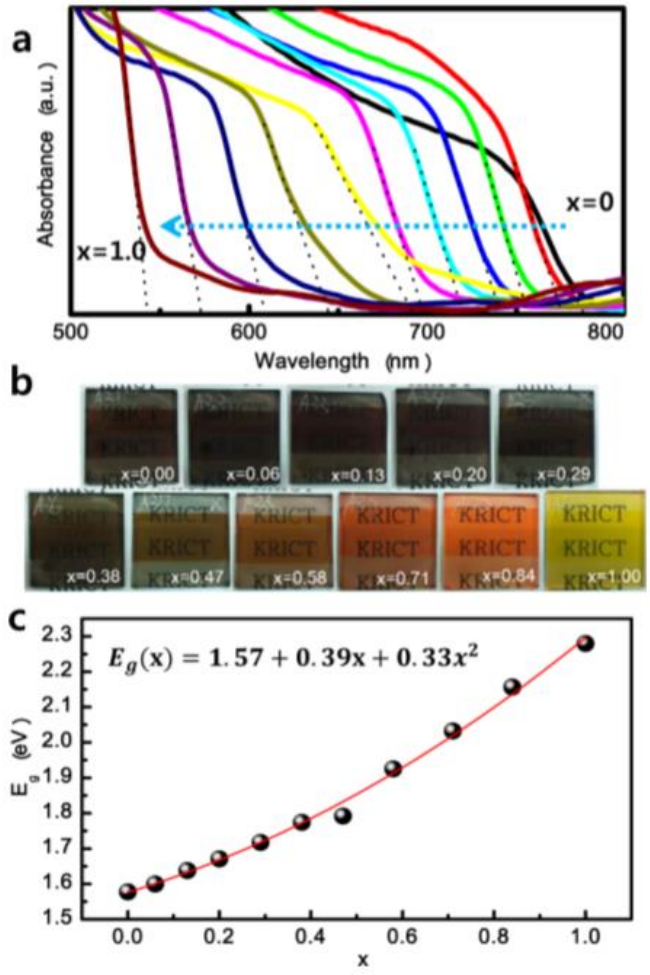

Figure 8: a) Uv-vis absorption spectra of $MAPb(I_{1-x}Br_x)_3$ b) Photographs of the perovskite alloys on mesoporous TiO_2 on FTO glass substrates. c) A quadratic relationship of the bandgap and the bromide ratio[33].

A few months after these observations, also the tunability of $MAPbI_3$ bandgap through addition of Cl^- was tested[35]. However, the large difference in Cl-I ionic radii hinders formation of the alloy at high Cl^- ratios, so that only films with low Cl^- ratio could be prepared from solution[35], vapor-assisted solution deposition[37] and coevaporation[34]. The low incorporation of Cl^- in the $MAPbI_3$ structure was determined by XRD spectra, which indicated the presence of $MAPbCl_3$ phase and no shift of the main peak of $MAPbI_3$. Even though the bandgap of these Cl^--doped $MAPbI_3$ films remains the same, as calculated from Tauc plots, charge transport increases dramatically, and this is the reason why other attempts have been made to dope a perovskite with another perovskite with lower HOMO.

The optical properties of the Br analogue $MAPbBr_{3-x}Cl_x$ were studied when the applications of perovskites in optoelectronic devices were still unknown[38]. From XRD spectra observations, it is clear that the combinations of these two anions results in an alloy and not in a two phase system. Indeed, the peaks indicate just a constant decrease in lattice parameters as the concentration of

chloride increases, because of its smaller radius compared to that of the bromide. The bandgap was measured from optical absorption spectra and shifted from 2.35 eV to 3.11 eV by going from the pure bromide perovskite to the pure chloride perovskite.

$MAPbX_3$, polyanions perovskites.

A more recent study investigated the optical properties of $CH_3NH_3PbI_{(3-x)}(BF_4)_x$[39], where BF_4^- was used in order to take advantage of the electronic properties of F^- and avoid the problem of the different size of iodide and fluoride. In order to confirm the presence of BF_4^- in the structure, they carried out ATR-FTIR measurements. The bandgaps were measured from diffused reflectance spectroscopy followed by Tauc plots and they appear to be almost the same as the bandgap of pure $CH_3NH_3PbI_3$. This could be due to the almost same ionic radius of I^- and BF_4^-. In this case, the role of BF_4^- can be compared to that of boron in silicon solar cells.

Another mixed form with a different polyanion, namely SCN^-, was studied in order to investigate its influence on the stability of $MAPbI_3$[40]. In this case, the perovskite under study was $MAPbSCN_2I$, and the bandgap was calculated from reflection spectra and Kubelka-Munk function. The bandgap of iodide perovskite was measured to be 1.504 eV while that of the mixed form 1.532 eV. The slightly higher bandgap of the mixed form could be due to the larger ionic radius of the thiocyanate ion 2.15/2.20 Å[41] vs 19.8 Å of the iodide and to its slightly bigger electronegativity[42].

$FAPbX_3$, formamidinium halide perovskites.

As for the methylammonium perovskites, also for the formamidinium ones a study about the mixed halide forms was carried out[43]. The bandgaps of $FAPbI_xBr_{3-x}$ were extracted from Tauc Plots using data taken from absorption spectra and confirmed by photoluminescence measurements in order to discard the possibility that the absorption onsets were due to trap or sub-band states. The bandgap was tuned from 1.48 eV to 2.23 eV going from x = 3 to x = 0.

Discussion.

The experimental results discussed above matched the computational studies from which it was possible to extract the correlations between the bandgap change and the electronegativity and size of the X component. Indeed, by replacing the iodide with a more electronegative halide, it was shown that the bandgap broadens and this trend is evident also in mixed halide perovskites. However, some discrepancies between different studies should be discussed more in detail in order to understand where these differences come from. For instance, in one study[32] the bandgap of $MAPbI_{2.1}Cl_{0.9}$ was measured, even though other studies[34,35,37] demonstrated that it is not possible to synthesise mixed iodide/chloride perovskites with such a high chloride ratio. However, in the same study[32], they also carried out XPS measurements to determine the real I:Cl ratio in the products and they found out that when the stoichiometric ratio of I:Cl was 2:1, the real ratio was 1:0. Therefore, they referred to the stoichiometric ratio rather than the real I:Cl ratio. The value of the bandgap for this perovskite is still much higher than that of the pure iodide one (2.60 eV vs 1.52 eV) and this result is in disagreement with other observations[37] (1.58 eV vs 1.53 eV). What distinguishes these two studies, in addition to the different synthetic routes used to prepare the samples, is the way in which they extracted the bandgap. Indeed, they both used Tauc plots but the first study[32] considered that the absorption coefficient is proportional to the square of the energy while the second study[37] considered that it is proportional to the square root of the energy. This difference arises from considering the bandgap of the perovskite indirect, in the first case, and direct in the second case. Most of the studies consider it

to be direct and use the second correlation to draw Tauc plots. However, the nature of the perovskite's bandgap is still under debate[44].

With regard to the $MAPb(I_{1-x}Br_x)_3$ study[33], in which they shown a linear correlation between the bandgap and the bromide content, they incorrectly extracted the bandgap values directly from the absorption spectra instead of using Tauc plots.

Chapter 3. The inorganic cation

The B cation strongly contributes to both the valance and the conduction band, so that the VBM and CBM can be said to have an intra-atomic B character. This is the reason why, even when replacing the iodide with other more electronegative halide, the difference in the bandgap is not as large as expected. Moreover, it might be also the reason why these direct-bandgap semiconductors show very strong absorption and photoluminescence intensities[30].

The most studied divalent B cation is Pb^{2+} and it has been also the one with which the highest efficiencies of perovskite solar cells have been reached so far[17]. However, it is a toxic element, which is a factor that could hamper the commercialization of perovskite cells because of concerns due to its possible bioaccumulation in ecosystems and risk for human health. For this reason, some attempts to replace lead with another divalent metal have been made over the last years.

The closest element to Pb in the periodic table that could replace it in the perovskite structure is Sn. However, Sn perovskites are not stable in air[45] and for this reason mixed Pb-Sn perovskites have been the subject of considerable research[45,46,47,48]. Experimentally, the bandgap of $MAPbI_3$ has been measured from optical spectroscopy to be 1.54 eV, while that of $MASnI_3$ 1.20/1.28 eV, depending on the synthetic procedure[45]. In order to explain these values and how the valance and the conduction band energies change when Pb^{2+} is replaced by Sn^{2+}, simulations were carried out[49]. It was found that the spin-orbit-coupling-GW (SOC-GW) method was the one leading to the results closest to the ones experimentally measured. $MAPbI_3$ and $MASnI_3$ have both a tetragonal crystal structure at room temperature[47] but since Sn is smaller than Pb, the B-X distance in the first case is shorter than in the latter. Therefore, the difference in bandgap can be attributed to two different factors, namely the structural and the electronic factor. The first one was determined by doing the calculations for the two perovskites considering the same lattice parameters. There was still a difference in the bandgap but lower than the real one, and this reduction was thus due just to structural differences. The electronic factor is mostly due to the difference in energy between the Sn 5s and the Pb 6s orbital. Indeed, the latter has a lower energy than the former because of relativistic effect. Its lower energy makes its interaction with the p orbitals of the iodide weaker so that the antibonding orbital generated from this interaction and that forms the VBM is less destabilized, namely at lower energy. The CBM, which is mostly formed by B p orbitals, has also a lower energy when B = Pb, but to a lesser extent than the VBM, so that the overall effect of shifting from Pb to Sn is a reduction of the bandgap.

In the other chapters it was possible to observe logical correlations between the bandgap and the components 'properties, such as the size or the electronegativity. In the case of the metal cation, the problem is more complicated so that simplified correlations cannot be given. Indeed, the cations that were investigated do not belong either to the same group of the periodic table[46,50] and possess different properties that can be originated by more complex factors due to their heavy metal nature, such as spin-orbit coupling.

Current state of the art.

<u>One B component perovskites.</u>

The optical bandgap of $FASnI_3$ was calculated from the onset of the absorbance spectrum and is 1.41 eV, slightly smaller than that of $FAPbI_3$ (1.48 eV)[45]. As previously touched upon, $MASnI_3$ shows a different bandgap depending on the synthetic approach employed while $MAPbI_3$ did not present this behaviour. A big difference between these two perovskites is that the latter is more stable in air than the other one. Therefore, one possible explanation to this change in bandgap with different conditions

is that depending on the environment in which the perovskite is synthesised and stored, it can be more easily oxidized, so that the final product is not pure $MASnI_3$ but a compound in which some Sn^{2+} was oxidized to Sn^{4+}. The oxidized compound has, of course, a different bandgap than $MASnI_3$.

Mixed Sn/Pb perovskites.

Mixed Sn/Pb methylammonium iodide perovskites have been synthesised and characterized by different research groups, but curiously they all obtained different values of the bandgap[46,47,48]. Indeed, one group[47] carried out research about solar cells made with perovskites deposited on mesoporous TiO_2 with formula $CH_3NH_3Sn_xPb_{1-x}I_3$, and they found that by increasing the amount of tin the bandgap drops. Figure 9 shows the absorbance spectra of the samples and the table below the extracted bandgaps from the absorption spectrum edges and the XPS verified formula. The reason why the iodide ratio is lower than expected for the more tin-enriched alloys is probably that these perovskites are more easily oxidized during the measurement.

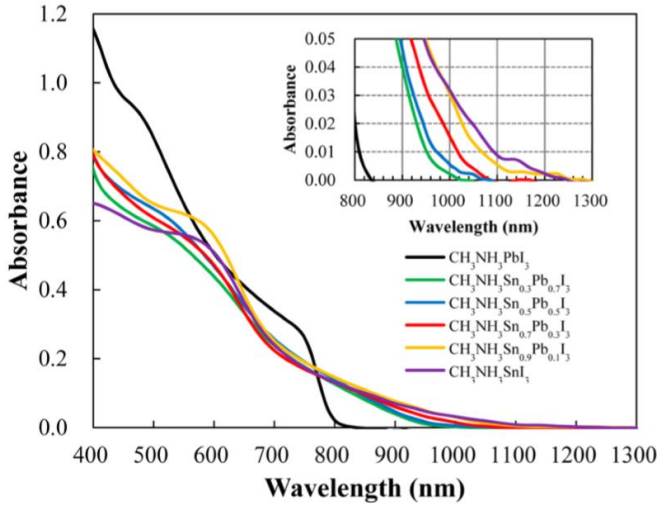

Figure 9: Electronic absorption spectra of $CH_3NH_3Sn_xPb_{(1-x)}I_3$ perovskite coated on porous TiO_2[47].

Stoichiometric formula	XPS verified formula	Eg (eV)
$CH_3NH_3PbI_3$	$CH_3NH_3PbI_{3.07}$	1.51
$CH_3NH_3Sn_{0.3}Pb_{0.7}I_3$	$CH_3NH_3Sn_{0.37}Pb_{0.63}I_{2.95}$	1.31
$CH_3NH_3Sn_{0.5}Pb_{0.5}I_3$	$CH_3NH_3Sn_{0.56}Pb_{0.44}I_{2.77}$	1.28
$CH_3NH_3Sn_{0.7}Pb_{0.3}I_3$	$CH_3NH_3Sn_{0.74}Pb_{0.26}I_{2.47}$	1.23
$CH_3NH_3SnI_3$	$CH_3NH_3SnI_{1.96}$	1.10

Table 2: Bandgaps of $MAPb_xSn_{1-x}I$. The second column shows the real Pb:Sn ratio measured from XPS analysis.

Another work[48], published also in 2014 as the previous one, found out that the bandgap of the mixed compounds deposited as thin films do not follow this linear trend but are narrower than the bandgaps of both the pure compounds. The values were extracted from the absorption spectrum edges determined from the conversion of diffuse reflectance measurements of the pure and mixed compounds and their values are listed in the table below. Also in this case, XPS analysis confirmed that the stoichiometric ratio was maintained. Moreover, they verified that Sn and Pb were homogenously distributed throughout the film via SEM energy-dispersive X-ray spectroscopy (EDS). In 2016, a similar trend was observed for mixed perovskite composed by $FA_{0.75}Cs_{0.25}Sn_{0.5}Pb_{0.5}I_3$[51].

Stoichiometric formula	Eg (eV)
$CH_3NH_3PbI_3$	1.55
$CH_3NH_3Sn_{0.25}Pb_{0.75}I_3$	1.24
$CH_3NH_3Sn_{0.5}Pb_{0.5}I_3$	1.17
$CH_3NH_3Sn_{0.75}Pb_{0.25}I_3$	1.17
$CH_3NH_3SnI_3$	1.30

Table 3: Bandgaps of $MAPb_xSn_{1-x}I$

In 2015, a third study[46] claimed that the $MAPb_{0.5}Sn_{0.5}I_3$ shown almost the same absorbance spectrum as $MAPbI_3$, as reported in figure 10, and justified the different result obtained by asserting that depending on the preparation method, both the crystalline phase and the optical properties got affected.

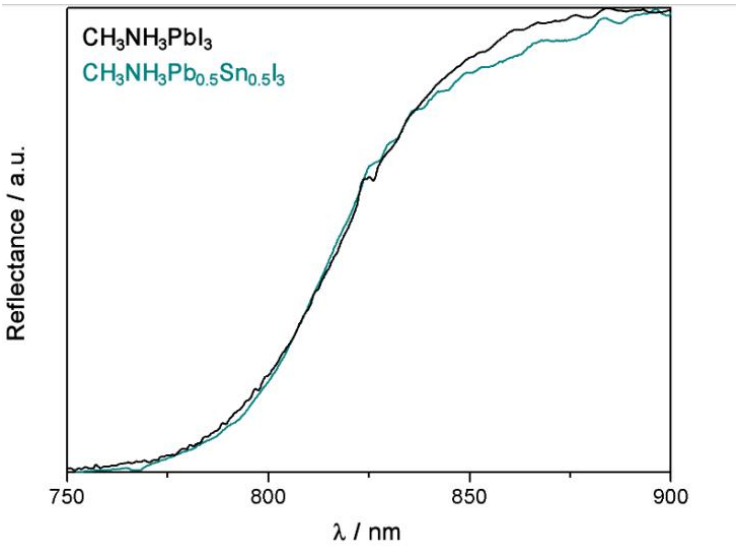

Figure 10: Reflectance spectra of $MAPbI_3$ and $MAPb_{0.5}Sn_{0.5}I_3$[46] (Supporting information).

Doped $CH_3NH_3PbI_3$ perovskites in Pb^{2+} sites.

A 2015 work[46] focused on the synthesis and characterization of $CH_3NH_3PbI_3$ perovskite doped in the B position with Sn^{2+}, Sr^{2+}, Cd^{2+} and Ca^{2+}. The ratio of dopant is varied from 0.05 to 0.15 and it was verified through XPS analysis. All the samples maintain their tetragonal structure except for the Ca^{2+} one, which shifts to the cubic phase. The bandgaps were calculated from Tauc plots of data taken from diffuse reflectance UV-Vis spectra and the ones of the samples with dopant ratio equal to 0.1 are reported in figure 11.

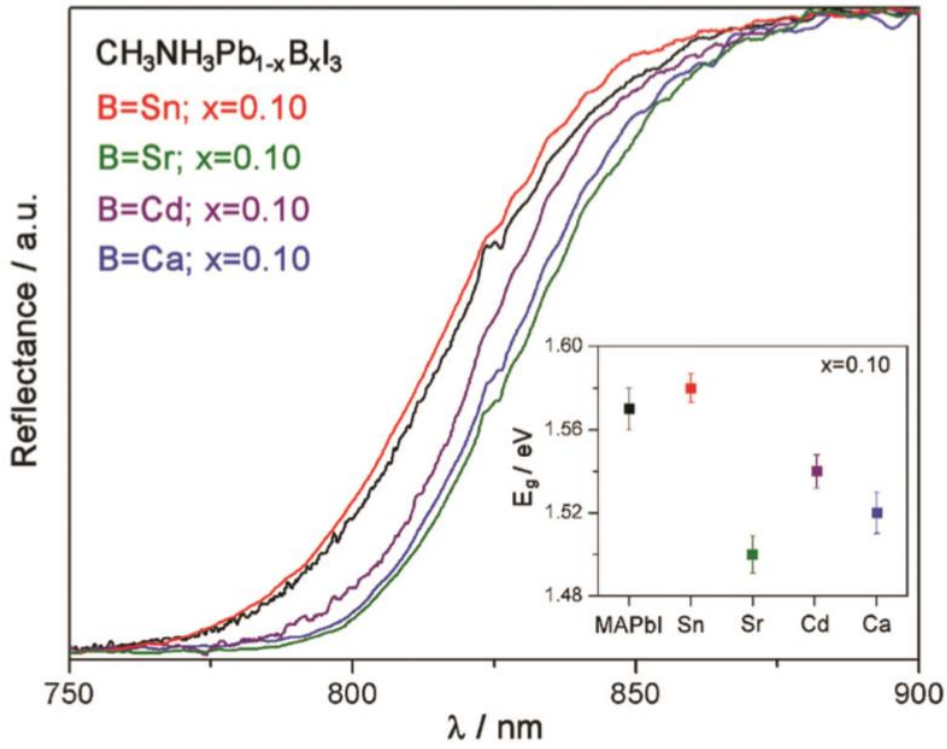

Figure 11: Diffuse reflectance UV-Vis spectra for the MAPbI3 sample, and MAPb1−xBxI3, with B = Sn2+, Sr2+, Cd2+, Ca2+, and x = 0.10. In the inset, the plot of the optical bandgap values for each sample[46].

As shown in the inset of the figure, the only doped perovskite showing a higher bandgap than the pure form is the Sn one. However, the table below shows the optical bandgap values that were extracted from the reflectance spectra of all the samples and it seems that this increase occurs only at this precise concentration.

Optical band gap values for the samples synthesized

$MAPb_{1-x}B_xI_3$			$MAPb_{1-x}B_xI_3$		
B	x	E_g/eV	B	x	E_g/eV
—	0.00	1.57	Cd	0.05	1.54
Sn	0.05	1.57		0.10	1.54
	0.10	1.58		0.15	1.54
	0.15	1.57	Ca	0.05	1.52
Sr	0.05	1.51		0.10	1.52
	0.10	1.50		0.15	1.52
	0.15	1.51			

Table 4: Bandgaps of $MAPb_{1-x}B_xI_3$

Lead- Free perovskites

Recently, a completely lead-free perovskite solar cell has been engineered. The lead-free perovskite has formula $MA_2CuCl_xBr_{4-x}$ and has a 2D structure because of the relatively small ionic radius of Cu^{2+} (73 pm) and it is also stable in air thanks to the high stability of Cu^{2+} in this oxidation state and

to the presence of chloride. From absorption spectra and the corresponding Tauc plots, the estimated bandgaps were 2.48 eV for MA_2CuCl_4, 2.12 eV for $MA_2CuCl_2Br_2$, 1.90 eV for $MA_2CuClBr_3$ and 1.80 eV for $MA_2CuCl_{0.5}Br_{3.5}$. As predictable, when the ratio of bromide increases the bandgap drops.

Discussion.

The contradictions shown by the different studies on mixed Sn/Pb perovskites highlight many interesting points of discussion about the bandgap determination. The first two studies[47,48] did not use the Tauc plots to extrapolate the bandgap from the optical experiments but looked directly at the absoption edge. In this way, they did not take into account that for direct bandgap semiconductor the correlation between the absorption coefficient and the energy is not linear but quadratic. The third study[46] extrapolated the bandgap value properly from Tauc plots and data taken from diffuse reflectance spectroscopy, but did not verify whether the ratio of Pb/Sn in the product corresponded with the stoichiometric one. Lack of inclusion of Sn in the final product would explain why it was found that $MAPb_{0.5}Sn_{0.5}I_3$ has the same optical properties as $MAPbI_3$.

In general, it might be argued that when the bandgap changes depending on the method used to prepare the perovskite film, the difference in bandgap has to be correlated not only to a difference in the preparation method but mainly to a difference in the composition of the final product, difference that can be ascribed to a different synthetic route. For instance, the degree of oxidation of Sn^{2+} in Sn^{4+} in the final product must depend on the synthesis and on the environment in which it was carried out and in which the perovskite was handled afterwards.

Moreover, it has been argued[52,53] that the bandgap of perovskites depends also on the size of the crystallites, which changes when the perovskite is deposited on mesoporous scaffolds, such as in the first study[47], and when it is prepared as thin film, as in the second study[48].

Chapter 4. The organic cation

This chapter deals with the interactions between the organic cation and the inorganic framework. These interplays influence the overall structure of the crystal and the physical and chemical properties of the perovskite. An overview of the results obtained through simulations and experimental work over the last few years is presented in order to determine general features that characterize the dependence of the perovskite's bandgap on the nature of the organic cation. The second part of the chapter focuses on state-of-the-art experimental findings that have not yet been rationalized but contribute to enhancing the stability or the efficiency of perovskite-based solar cells.

Influence on X-B-X angles.

It has been demonstrated through simulations[54,55], in addition to experimental evidence[45,43], that the value of the metal-halide-metal bond angles and the metal-halide bond length influence the electronic and optical properties of the perovskite, the bond angles more so than the bond length[55]. These values are strongly affected by the size and the nature of the organic cation, so that, the choice of the latter can be used to modulate the bandgap. This is very interesting since the lowest bandgap reachable by replacing the X component in $MAPbX_3$ perovskites is about 1.6 eV when using the iodide ion[56], still far from the optimal bandgap for reaching the Shockley-Queisser limit[23], around 0.2 eV lower.
Figure 12 depicts how the two metal-halide-metal angles decrease when the archetypical cubic structure distorts. When the organic cation is sufficiently large to fill the cubooctahedral cage between the 12 nearest X atoms, these distortions are hindered, so that the angles tilt to a lesser extent.

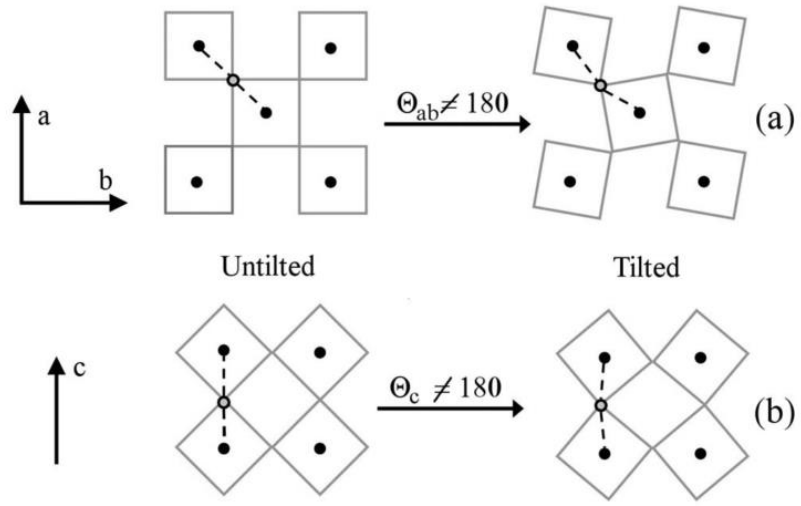

Figure 12: Comparison between an untilted cubic configuration and the tilted orthorhombic one in the ab plane (a) and along the c axis (b)[54].

In a 2014 study on steric engineering of metal-halide perovskites[55], starting from the observation that the organic cation does not strongly influence the energy of the frontier orbitals, they calculated the bandgap of a "Platonic" metal-halide structure, consisting in a regular polyhedron,

that does not contain organic cations but just PbI_6 octahedra that share the corners regularly. They used DFT (density functional theory) and calculated how the bandgap changes as a function of the two halide-lead-halide angles, namely the one along the apical direction and the one along the equatorial direction. In their calculations the Pb-I length value was kept constant (3.18Å), while the angles were shifted from 120° to 180°. The results, shown in figure 13, clearly demonstrate that the angles distortions can be used to modulate the bandgap of the perovskite.

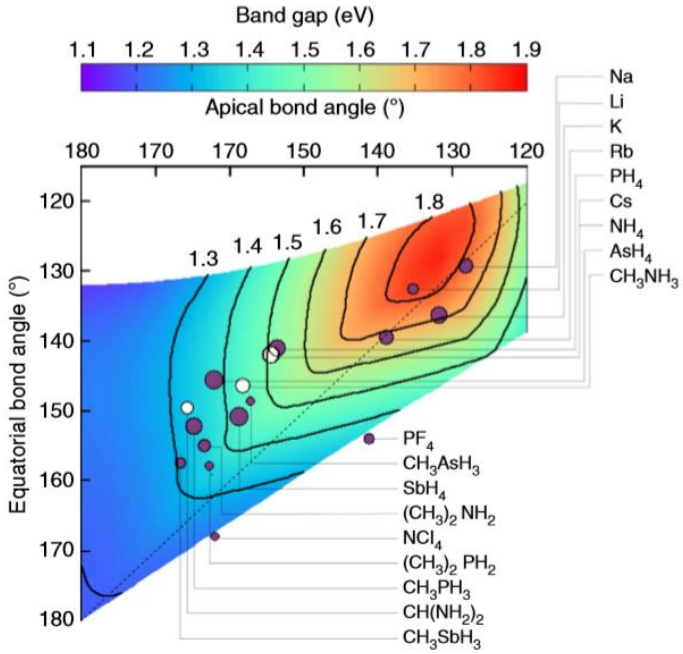

Figure 13: Representation of the change in DFT bandgap depending on the value of the apical and equatorial metal-halide-metal bond angles. The plot shows also which A cation would generate those specific B-X-B angles and the white discs indicate the cations that have already been used experimentally. The dashed line is just a guide to the eye to highlight that the plot is almost symmetric[55].

Figure 13 indicates also which organic or inorganic cations would give rise to those angular distortions and differentiates the perovskites that have already been synthesised from those that have not. The main feature is that the bandgap increases as the angles tilt. The reason for this trend can be derived from looking at the conduction band formation from the atomic orbitals. Indeed, when considering the most symmetric structure, the one corresponding to the situation depicted in the bottom left in figure 13, the conduction band results from the overlap of collinear orbitals, while by shifting towards lower angles this overlap occurs more and more as a pi (π) interaction and the energy of the level increases, because of this decreased overlap. The overall result is an increase in the bandgap. The main conclusion of this study is that the tilt of the optimal angles influences the bandgap and the size of the organic cation can be used to control this tilting. The next step to engineering new perovskites with optimal bandgap is to consider many compounds, which have something in common with the most used ones, and calculate the bandgap of the correspondent perovskite. Figure 14 shows the cations that have been investigated together with the resulted perovskite bandgap. As predicted, the latter decreases by increasing the cation size.

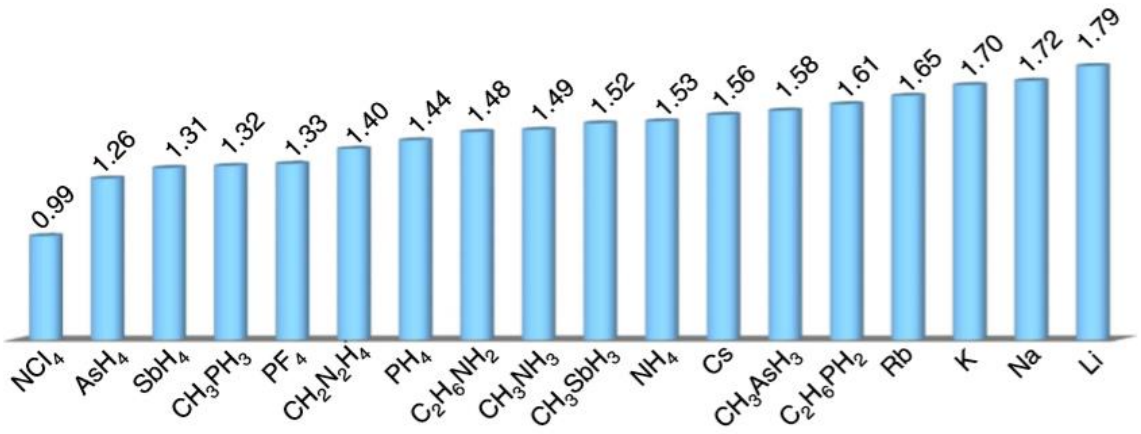

Figure 14: Calculated bandgaps of PbI_3-based perovskites[55].

In general, the size of the organic cation influences also the B-X bond length and it was demonstrated through simulations that larger cations deliver smaller band-gaps[54]; however, this has been considered a second-order effect[55] compared with that of the tilted angles deviations.

Influence through H bondings.

The theoretical correlation between the perovskite bandgap and the cation size has been widely confirmed by experimental data. Indeed, when in the perovskite $CH_3NH_3PbI_3$, the methylammonium (MA), which has an effective radius of 217 pm[27], is replaced by the slightly bigger cation $CH(NH_2)_2^+$ (FA), the formamidinium ion, whose radius measures 253 pm[27], the bandgap decreases from around 1.6 eV to around 1.5 eV. Besides, similar results have been found by substituting MA with Cs^+, which has a smaller radius, namely 188 pm[15], the resulting bandgap being higher, namely 1.73 eV[57].

Even though these results seemed to confirm the correlation between the cation size and the bandgap, some differences appeared too significant to be due to only the small difference in size. In fact, the difference in size between MA and FA is not that large to justify the different geometry of crystallization, tetragonal for $MAPbI_3$ and trigonal for $FAPbI_3$. This difference suggested that probably, together with the size, something else occurs when changing the organic cation. Effectively, the interaction between the organic cation and the inorganic counterpart changes as A is replaced, because new H bonds are involved. While in MA there are only three acidic hydrogen atoms that can interact with the halide, FA contains four hydrogens (figure 15).

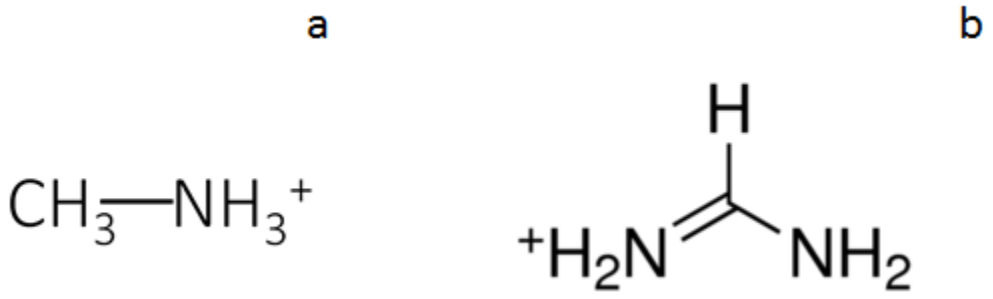

Figure 15: Lewis structures of methylammonium (a) and formamidinium (b).

As the number of hydrogen bonds with the halide increases, the nature of the Pb-I bond gets more and more ionic, with a greater negative charge on the halide and a more positive one on the lead cation. The contribution of lead in the valance and conduction bands increases as the bond becomes more ionic. This behaviour has been correlated with an increase in spin-orbit coupling, which indeed plays a bigger role when heavier elements are involved. In absence of spin-orbit coupling (SOC), the bandgap of $MAPbI_3$ and $FAPbI_3$ would be very similar, even though they assume different crystal structures. However, when taking into account the SOC, bandgaps very close to the experimental ones have been calculated. This demonstrates that the decrease in the bandgap is not due just to the size difference between MA and FA[28].
Computational work based on this theoretical explanation matched experimental results[28].

Current state of the art.

Perovskites with one A component.
Since halide perovskites started to be a hot research topic, many combinations of materials have been tested in order to enhance the overall efficiency of perovskite-based solar cells by increasing the light harvesting and the conductivity of the material. Not only perovskites with organic cations other than **methylammonium** were synthesised, but also mixed forms of organic cations and combinations of organic and inorganic cations.
Despite the high efficiencies that have been reached with $MAPbI_3$ in solar cells, some challenges have been reported, namely:

- $MAPbI_3$ bandgap is higher than the optimal bandgap to reach the Shockley-Queisser limit of about 0.2 eV[56].
- It is sensitive to moisture, therefore unstable in air[17],
- It undergoes a reversible phase transition from cubic to tetragonal phase at 57°C[31], that falls within the device operating temperatures. This change affects the bandgap and the stability of the material.

Starting from the structural consideration done above, namely bearing in mind the correlation between cation size and bandgap, Nam-Gyu Park et al.[9] reported the synthesis of a lead iodide perovskite where the methylammonium was replaced by the bigger **ethylammonium**. In this case, instead of obtaining a lower bandgap perovskite as expected, since the organic cation was too large to maintain a 3D lattice structure, the structure shifted to a 2D structure. The optical bandgap that resulted was 2.2 eV, much higher than that of the methylammonium iodide perovskite.
The **formamidinium** ion, on the contrary, being slightly bigger than methylammonium, fits well in the 3D structure so that, as predicted from the previous analysis, $FAPbI_3$ has a lower bandgap

than $MAPbI_3$, namely 1.47 eV. This bandgap was calculated from the Tauc Plot of the perovskite deposited on quartz substrate[58]. Many synthetic routes have been reported for this perovskite[58,59,60,61] and depending on how it was prepared and of course on the structure of the engineered device, efficiencies up to 20% were reached[61]. An illusory advantage of formamidinium to the methylammonium ion is that the first exhibits thermal stability because the thermal transition does not occur at device operation temperatures[60]. However, the black low bandgap $FAPbI_3$ perovskite shows a yellow polymorph with a larger bandgap at temperatures lower than 60 °C. This polymorph reduces the photovoltaic performances not only because of its lower light harvesting because of the bigger bandgap but also because it probably hinders electron transport[58]. Figure 16 depicts both the back and the yellow $FAPbI_3$ polymorphs.

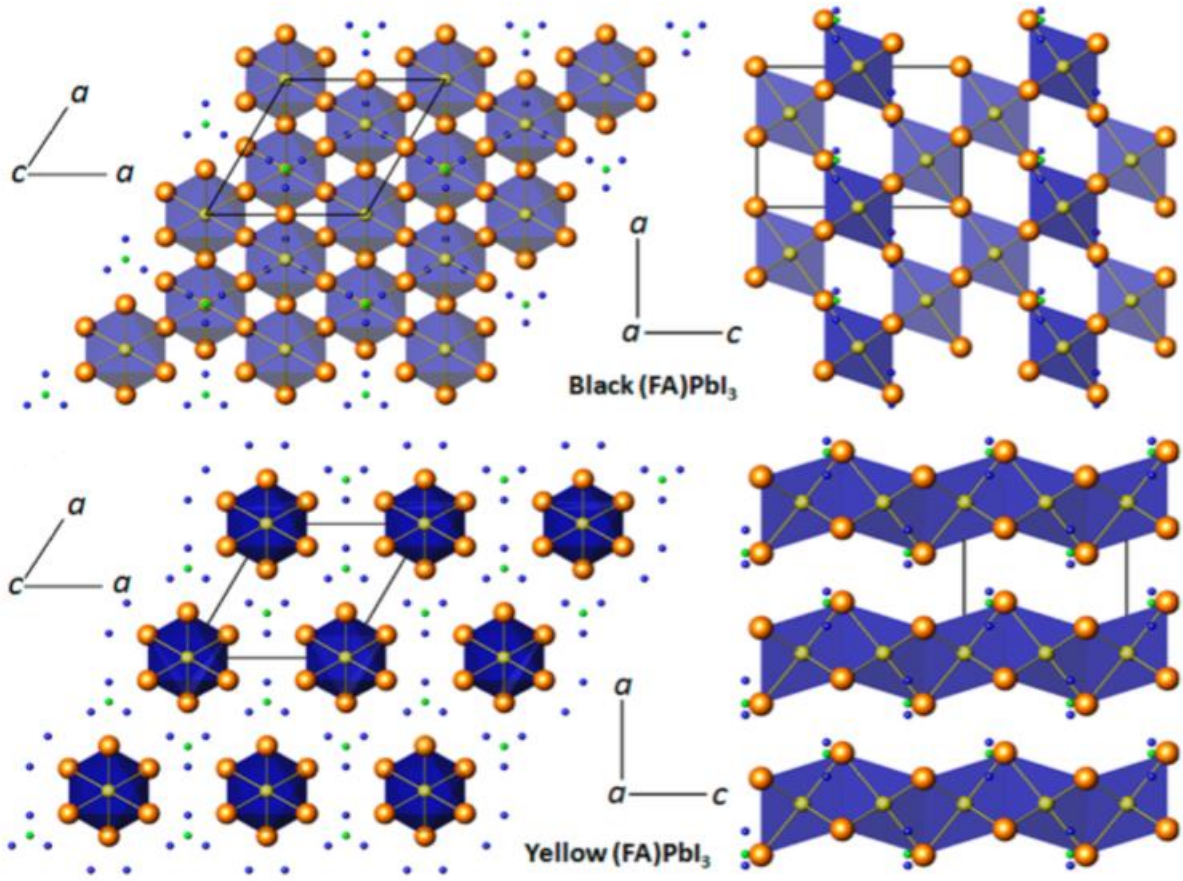

Figure 16: Representation of the two FAPbI3 polymorphs along the crystallographic c (left) and a (right) axes. The blue areas represent the inorganic octahedral PbI_6, while the organic cation is represented by the smaller blue and green dots[58].

The presence of these two forms, one of which does not show suitable optical properties for photovoltaic applications, pushed the scientific community to look for mixed organic cation forms that might combine the good carrier mobility of $MAPbI_3$ and the optimal bandgap of $FAPbI_3$. Later on, these attempts are described. To conclude the discussion about the FA cation, it has a lower dipole moment than MA[28], factor that could be important in contributing to hysteresis if assumed that the latter depends on the dipole moment of the A cation.

Regarding this last observation, the **guanidinium** (GA) ion, depicted in figure 17, drew great interest because of its symmetry, which theoretically determines a zero dipole moment, so that the hysteresis might be reduced[62]. However, it is too large (278 pm[63]) to fit in the cavity between the octahedra. An experimental study[63] shown that the bandgap of mixed $MA/GAPbI_3$,

extrapolated from Tauc plots, changes with the GA/MA ratio just slightly, namely between 1.53 and 1.55 eV and that GA does not directly replace MA in the crystal structure.

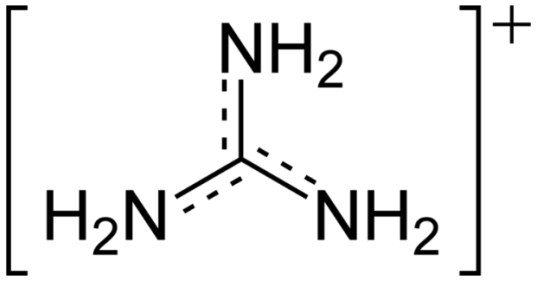

Figure 17: Lewis structure of guanidinium ion.

Mixed organic perovskites.

As suggested previously, the perovskites made from single organic cations suitable for photovoltaic applications show drawbacks that have not been overcome after few but intense years of research. First of all $MAPbI_3$ undergoes a phase transition within the temperature range of device operation. Secondly $FAPbI_3$ shows two polymorphs below 60 °C. Thirdly, $CsPbI_3$ is more stable than the organic alternatives but has a too high bandgap for being a satisfying alternative to the hybrid forms. For this reason, over the last three years, mixed cation perovskites have been investigated. They have impressively shown higher performance than the pure forms. Indeed, particular combinations of the most common cations allow the drawbacks of instability or high bandgap to be avoided.

The first study on the optical and photovoltaic properties of mixed $MA_xFA_{1-x}PbI_3$ perovskites as light-harvesting pigments in mesoscopic solar devices was carried out in 2014 and shown noteworthy results[64]. Indeed, the overall efficiency of the cell was higher than both the pure MA and FA cells. What is remarkable about this study is that the bandgap of the mixed form with MA:FA = 3:2 was measured to be equal to the bandgap of the pure formamidinium iodoplumbate, namely 1.530 eV, slightly lower than that of the MA equivalent, namely 1.575 eV. The bandgaps were calculated from the onset of the absorption spectra measured with an integrating sphere and they are rather different from those calculated or measured with different techniques.

Other mixed organic forms have been tested for a different purpose, namely in order to modify the crystal arrangement of the perovskite film on mesoporous materials. Indeed, as for the ethylammonium case, when MA is partially replaced by 5-aminovaleric acid cations (5-AVA) in $APbI_3$, these bigger cations do not fit in the cubooctahedral cage and thus, produce a layered structure composed by alternated inorganic PbI_6 octahedra and organic layers[65]. The latter are probably formed by 5-AVA cations that bind to each other through hydrogen bonds as it was reported for the case of 4-ammonium-butyric acid (4-ABA) in mixed cation $(4\text{-ABA})_2MAPb_2I_7$ perovskite[66]. Figure 18 depicts the layered structure for the case of 4-ABA.

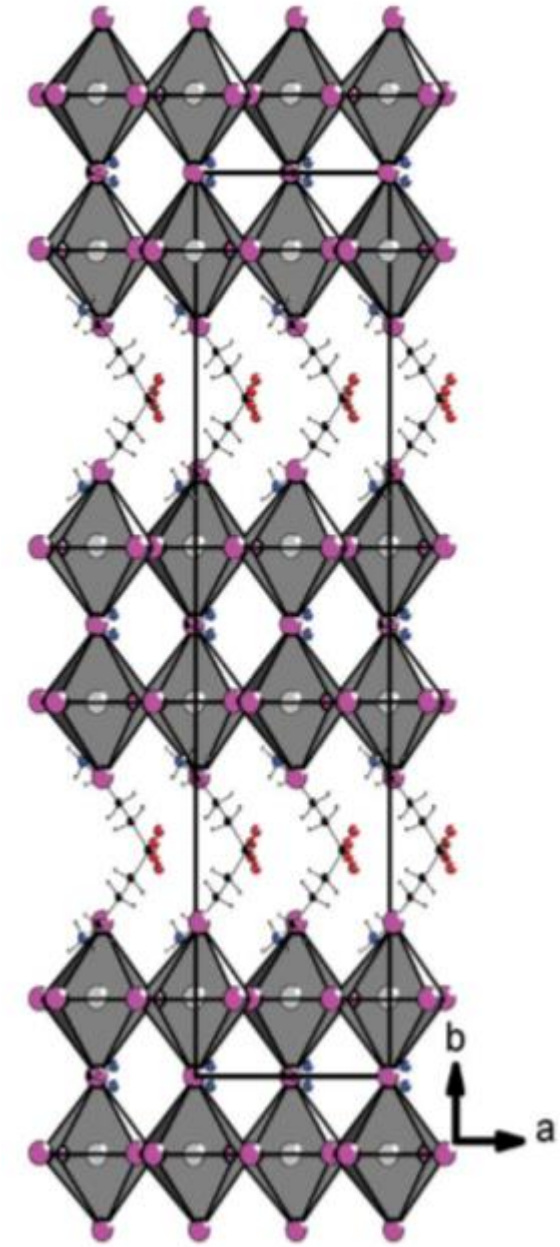

Figure 18: Layered crystal structure of $(HO_2C(CH_2)_3NH_3)_2(CH_3NH_3)Pb_2I_7$

Mixed organic-inorganic perovskites

The combination of organic and inorganic cations has also been the subject of some studies, for instance, the doping of $MAPbI_3$ with Cs^{2+} [67]. It was demonstrated that, with a 10% Cs^{2+} doping of $MAPbI_3$, even though the bandgap was higher than the pure MA perovskite, light absorption was increased over the whole solar spectrum. Indeed, as shown in figure 19, as the fraction of caesium increases, the bandgap broadens but at the same time the shape of the absorption spectrum changes. The presence of Caesium increases the amount absorption in the range of 300-400 nm while reduces the absorption between 450 and 800 nm. The highest light absorption is achieved via 10% Cs doping in the $MAPbI_3$ perovskite structure. To confirm that the Cs was homogeneously distributed on the film, they carried out elemental mapping using energy dispersive spectroscopy (EDS). Moreover, they checked the morphologies of the films through scanning electron microscopy and atomic force microscopy images and found out that they were smooth and they completely covered the substrate.

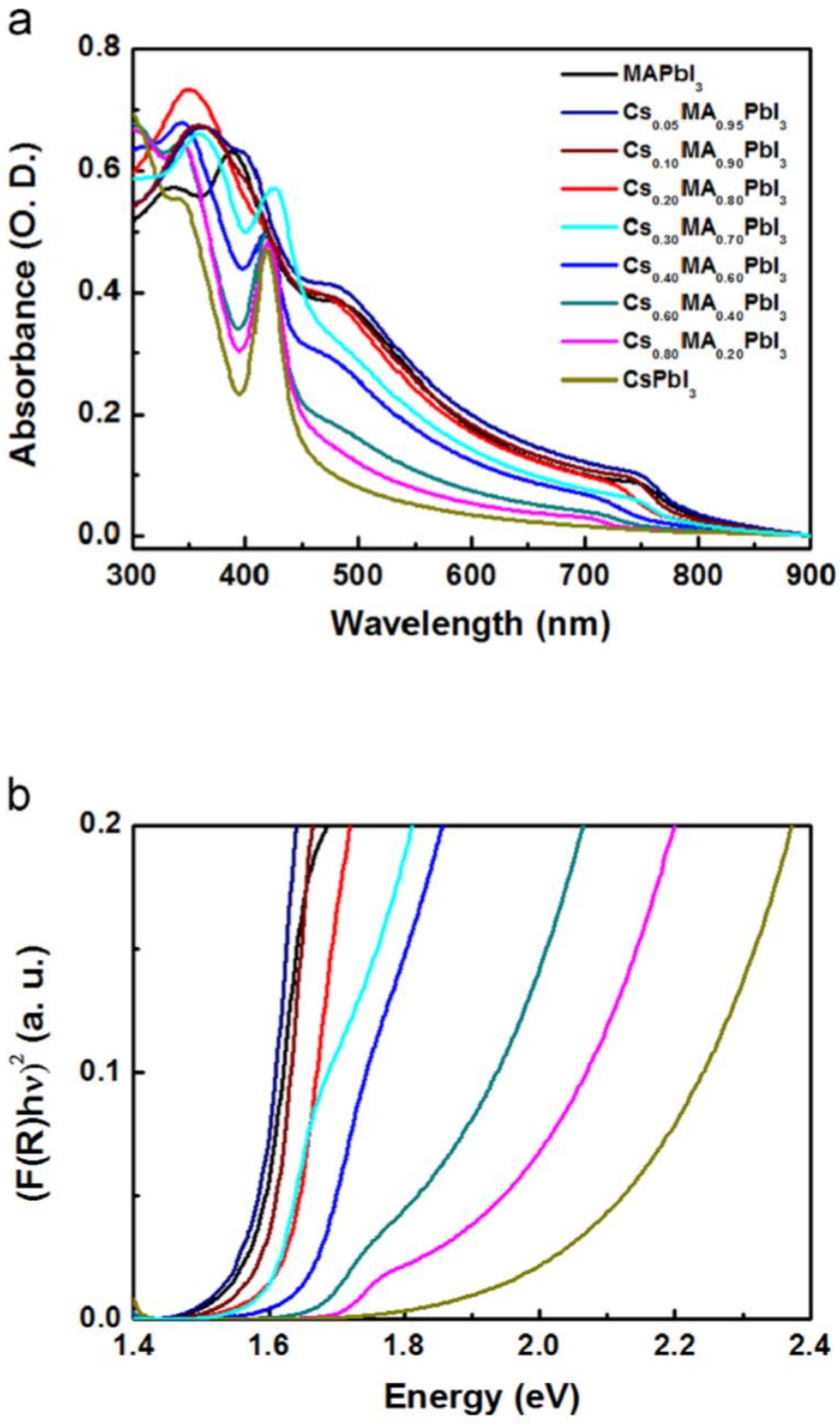

Figure 19: (a) UV–vis absorption and (b) transformed Kubelka–Munk spectra of $Cs_xMA_{1-x}PbI_3$ perovskite films with different Cs ratio[67].

One study[68] on triple cation perovskites was carried out with the purpose of enhancing the stability of the black polymorph $FAPbI_3$ in order to maintain the low bandgap and avoiding the instability. Even though the Cs doping decreases the light harvesting, as shown in figure 20, where the ratio

MA:FA is constant, the stability of the perovskite is increased. This was demonstrated by measuring the change in the device efficiency under operational conditions over time.

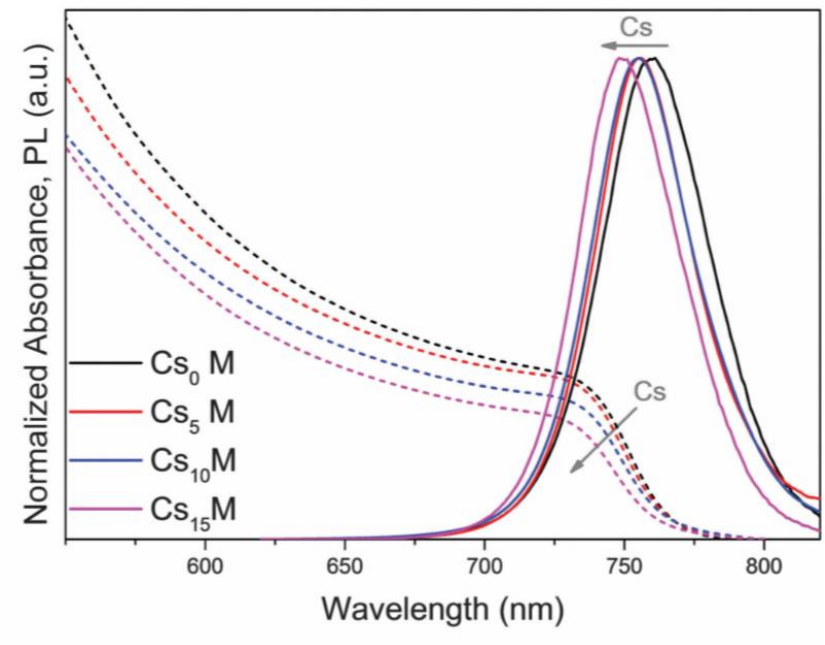

Figure 20: The absorbance (dashed lines) and photoluminescence (PL) spectra (solid lines) of Cs_xM perovskites, where M = $(MA_{0.17}FA_{0.83})_{(1-x)}Pb(I_{0.83}Br_{0.17})_3$ [68] .

A study on CsPbI3.

After the success of hybrid organic-inorganic perovskites, some authors[69] wondered about the need for the big cation to be organic rather than inorganic. In order to compare the two materials, they used Cs^+ in place of MA in $APbBr_3$ perovskites. The iodide perovskite was not used because the caesium lead iodide was found not to have a perovskite structure at standard temperature and pressure. This is in and of itself a limit, since the perovskite with iodide instead of bromide have a lower bandgap, closer to the optimal one. However, the caesium perovskite showed more stability at the rise in temperature than the organic equivalent and also the devices prepared with this inorganic cation gave good efficiencies, showing that this inorganic perovskite could in principle play the role that is given to the hybrid ones.

Discussion.

The results obtained from simulations[55] give useful information and suggest directions for future research but they show also some differences with the experimental results. For instance, the ethylammonium lead iodide was expected to have a bandgap of 1.48 eV[55], slightly lower than that of $MAPbI_3$ because of its bigger radius. Experimentally, a bandgap of 2.2 eV was observed because it shows a 2D structure instead of 3D one.

Another aspect that would have been difficult to determine from simulations is the polymorphism of FA at high temperature. Moreover, it is clear that many other factors have to be considered in addition to the change in bandgap when preparing new perovskites, for instance the stability of the perovskite and the synthetic route to prepare it.

Conclusions

In this work, the influence of the perovskite components on the optical bandgap of this impressive material was analysed through a review of the most relevant computational and experimental studies done so far. The aim was to find correlations between the properties of the components and the way they affect the value of the bandgap.

The analysis of the electronic structure of the inorganic $CsSnX_3$ perovskite[30], where X is a halide, shows that the valance band maximum and the conduction band minimum have both B and X character. This means that the value of the bandgap is directly affected by a change in B or X. On the contrary, the A cation does not play a direct role in the formation of these two electronic bands but still influences the value of the bandgap by affecting the B-X interactions through its size and its interactions with the inorganic framework. In this way, the bandgap of $APbI_3$ can be theoretically tuned from 0.99 to 1.79 eV[55] by replacing A with cations of different sizes.

Experimental studies proved the correctness of the simulations and sometimes highlighted their limits. Moreover, some discrepancies between experimental studies were discussed and some comments about their possible origin were given at the end of each chapter and in the Appendix. However, since some fundamental properties of perovskites are still under debate, for instance whether or not it is a direct bandgap semiconductor, it is not possible to argue which of the methods used to determine the bandgap is the most correct one.

References

1. Snaith, H. J. Perovskites : The Emergence of a New Era for Low-Cost , High-. *J. Phys. Chem. Lett.* **4,** 3623−3630 (2013).
2. Weber, D. CH 3 NH 3 PbX 3 , ein Pb(II)-System mit kubischer Perowskitstruktur. *Z. Naturforsch* **1445,** 1443–1445 (1978).
3. Weber, D. & Perovskite, C. (x = 0-3), ein Sn (II) -System mit kubischer Perowskitstruktur. *Z. Naturforsch* 0–3 (1978).
4. Mitzi, D.B., Felid, C. A., Harrison, W.T.A., Guloy, A. M. © 19 9 4 Nature Publishing Group. *Nature* **369,** 467–469 (1994).
5. D . B . Mitzi , S . Wang , C . A . Feild, C. . A. . C. and A. . M. . G. Conducting Layered Organic-Inorganic Halides Containing -Oriented Perovskite Sheets. *Am. Assoc. Adv. Sci.* **267,** 1473–1476 (1995).
6. Kojima, A., Teshima, K., Shirai, Y. & Miyasaka, T. Organometal Halide Perovskites as Visible-Light Sensitizers for Photovoltaic. *J. AM. CHEM. SOC.* **311,** 6050–6051 (2009).
7. Kim, H. *et al.* All-Solid-State Submicron Thin Film. *Sci. Rep.* 1–7 (2012). doi:10.1038/srep00591
8. Etgar, L. *et al.* High Effi ciency Quantum Dot Heterojunction Solar Cell Using Anatase (001) TiO 2 Nanosheets. *Adv. Mater. 2012* **24,** 2202–2206 (2012).
9. Nh, C. H., Im, J., Chung, J., Kim, S. & Park, N. Synthesis , structure , and photovoltaic property of a nanocrystalline 2H perovskite-type novel. *Nanoscale Res. Lett.* **7,** 1–7 (2012).
10. Michael M. Lee, Joël Teuscher, Tsutomu Miyasaka, Takurou N. Murakami, H. J. S. Efficient Hybrid Solar Cells Based on Meso-Superstructured Organometal Halide Perovskites. *Science (80-.).* **338,** 643–648 (2012).
11. Etgar, L. *et al.* Mesoscopic CH 3 NH 3 PbI 3 /TiO 2 Heterojunction Solar Cells. *J. Am. Chem. Soc.* **134,** 17396−17399 (2012).
12. Bi, Y. *et al.* Charge Carrier Lifetimes Exceeding 15 μ s in Methylammonium Lead Iodide Single Crystals. *J. Phys. Chem. Lett.* **7,** 923−928 (2016).
13. Dong, Q. *et al.* Electron-hole diffusion lengths > 175 m m in solution-grown CH 3 NH 3 PbI 3 single crystals. *Science (80-.).* **347,** 967–969 (2015).
14. Green, M. & Ho-baillie, A. The emergence of perovskite solar cells. *Nat. Photonics* 506–514 (2014). doi:10.1038/nphoton.2014.134
15. Chonghea Li, Xionggang Lu, Weizhong Ding, Liming Feng, Y. G. and Z. G. Formability of ABX (3) (X = F , Cl , Br , I) halide perovskites. *Acta Cryst.* **B64,** 702–707 (2008).
16. Walsh, A. Principles of Chemical Bonding and Bandgap Engineering in Hybrid Organic − Inorganic Halide Perovskites. *J. Phys. Chem. C* **119,** 5755−5760 (2015).
17. Albero, J., Malik, A. R. & Garcia, H. Influence of the Composition of Hybrid Perovskites on their Performance in Solar Cells. *J. Mater. Chem. A* 4353–4364 (2016). doi:10.1039/C6TA00334F
18. Brittman, S., Adhyaksa, G. W. P. & Garnett, E. C. The expanding world of hybrid perovskites: materials properties and emerging applications. *MRS Commun.* **5,** 7–26 (2015).

19. Ong, K. P., Goh, T. W., Xu, Q. & Huan, A. Structural Evolution in Methylammonium Lead Iodide CH 3 NH 3 PbI 3. *J. Phys. Chem. A* **119,** 11033−11038 (2015).

20. Oku, T. Crystal Structures and Related Perovskite Compounds Used for Solar Cells. *Sol. Cells - New Approaches Rev.*

21. Li, W. *et al.* Mechanical Tunability via Hydrogen Bonding in Metal − Organic Frameworks with the Perovskite Architecture. *J. Am. Chem. Soc.* **136,** 7801−7804 (2014).

22. Glaser, T. *et al.* Infrared Spectroscopic Study of Vibrational Modes in Methylammonium Lead Halide Perovskites. *J. Phys. Chem. Lett.* **6,** 2913−2918 (2015).

23. Shockley, W. & Queisser, H. J. Detailed Balance Limit of Efficiency of pn Junction Solar Cells. *J. Appl. Phys.* **32,** (1961).

24. Li, C., Chi, K., Soh, K. & Wu, P. Formability of ABO 3 perovskites. *J. Alloys Compd.* **372,** 40–48 (2004).

25. Giaquinta, D. M. Structural Predictions in the AB03 Phase Diagram. *Chem. Mater.* **6,** 365–372 (1994).

26. W. Travis, E. N. K. Glover, H. Bronstein, D. O. S. and R. G. P. Chemical Science On the application of the tolerance factor to inorganic and hybrid halide perovskites : a revised. *Chem. Sci.* **7,** 4548–4556 (2016).

27. Article, E., Kieslich, G., Sun, S. & Cheetham, A. K. Chemical Science Solid-state principles applied to organic – inorganic perovskites : new tricks for an old dog †. *Chem. Sci.* **5,** 4712–4715 (2014).

28. Amat, A.; Mosconi, E.; Ronca, E.; Quarti, C.; Umari, P.; Nazeeruddin, Md. K.; Grätzel, M.; De Angelis, F. Cation-Induced Band-Gap Tuning in Organohalide Perovskites: Interplay of Spin-Orbit Coupling and Octahedra Tilting. *Nano Lett.* **14,** 3608 (2014).

29. Brivio, F., Walker, A. B. & Walsh, A. Structural and electronic properties of hybrid perovskites for high-efficiency thin-film photovoltaics from first-principles Structural and electronic properties of hybrid perovskites for high-efficiency thin-film photovoltaics from. *APL Mater.* **042111,** (2016).

30. Huang, L. & Lambrecht, W. R. L. Electronic band structure , phonons , and exciton binding energies of halide perovskites. *Phys. Rev. B* **165203,** 1–12 (2013).

31. Baikie, T. *et al.* Synthesis and crystal chemistry of the hybrid perovskite (CH3NH3)PbI3 for solid-state sensitised solar cell applications. *J. Mater. Chem. A* **1,** 5628 (2013).

32. Li, C. *et al.* Halide-Substituted Electronic Properties of Organometal Halide Perovskite Films : Direct and Inverse Photoemission Studies. *ACS Appl. Mater. Interfaces* **8,** 11526−11531 (2016).

33. Noh, J. H., Im, S. H., Heo, J. H., Mandal, T. N. & Seok, S. Il. Chemical Management for Colorful, E ffi cient, and Stable Inorganic − Organic Hybrid Nanostructured Solar Cells. *Nano Lett.* **13,** 1764−1769 (2013).

34. Kim, T. G., Seo, W., Kwon, H. & Won, J. Influence of halide precursor type and its composition on the electronic properties of vacuum deposited perovskite films †. *Phys. Chem. Chem. Phys.* **17,** 24342–24348 (2015).

35. Colella, S. *et al.* MAPbI 3 - x Cl x Mixed Halide Perovskite for Hybrid Solar Cells : The Role of Chloride as Dopant on the Transport and Structural Properties. *Chem. Mater.* **25,**

4613−4618 (2013).

36. Slotcavage, D. J., Karunadasa, H. I. & Mcgehee, M. D. Light-Induced Phase Segregation in Halide- Perovskite Absorbers. *ACS Energy Lett.* **1,** 1199−1205 (2016).

37. Sedighi, R., Tajabadi, F., Shahbazi, S. & Gholipour, S. Mixed-Halide CH3NH3PbI3¢xXx (X=Cl, Br,I)Perovskites: Vapor-Assisted Solution Deposition and Application as Solar Cell Absorbers. *ChemPhysChem* **14588,** 2382–2388 (2016).

38. Kitazawa, N., Watanabe, Y. & Nakamura, Y. Optical properties of CH 3 NH 3 PbX 3 (X = halogen) and their mixed-halide crystals. *J. Mater. Sci.* **7,** 3585–3587 (2002).

39. Nagane, S., Bansode, U., Game, O. & Ogale, S. CH3NH3PbI(3-x)(BF4)x: molecular ion substituted hybrid perovskite †. *Chem. Commun.* **50,** 9741–9744 (2014).

40. Jiang, Q. *et al.* Pseudohalide-Induced Moisture Tolerance in Perovskite. *Angew.Chem. Int.Ed.* **54,** 7617–7620 (2015).

41. Kawamura, K. *et al.* Effective Ionic Radii of NO2- and SCN- Estimated In Terms of the Bottcher Equation and the Lorentz-Lorenz Equation. *J. Phys. Chem.* **2321,** 5205–5208 (1982).

42. Neale, L. G., Neale, L. D. G. & Bonamy, A. F. Calculating group electronegativities using the Lewis-Langmuir equation Calculating group electronegativities using the revised Lewis – Langmuir equation. *J. Mol. Struct.* **639,** 151–156 (2003).

43. Eperon, G., Herz, L. M., Herz, L. M. & Snaith, H. J. Formamidinium lead trihalide : A broadly tunable perovskite for efficient planar heterojunction solar cells Energy & Environmental Science Formamidinium lead trihalide : a broadly tunable perovskite for e ffi cient planar heterojunction solar. *Energy Environ. Sci.* **7,** 982 –988 (2014).

44. Hutter, E. M. *et al.* Direct–indirect character of the bandgap in methylammonium lead iodide perovskite. *Nat. Mater.* **1,** (2016).

45. Stoumpos, C. C., Malliakas, C. D. & Kanatzidis, M. G. Semiconducting Tin and Lead Iodide Perovskites with Organic Cations: Phase Transitions, High Mobilities, and Near-Infrared Photoluminescent Properties. *Inorg. Chem.* 9019−9038 (2013).

46. Navas, J. *et al.* New insights into organic – inorganic hybrid. *Nanoscale* **7,** 6216–6229 (2015).

47. Ogomi, Y. *et al.* CH3NH3SnxPb(1−x)I3 Perovskite Solar Cells Covering up to 1060 nm. *J. Phys. Chem. Lett.* **5,** 1004–1011 (2014).

48. Hao, F., Stoumpos, C. C., Chang, R. P. H. & Kanatzidis, M. G. Anomalous Bandgap Behavior in Mixed Sn and Pb Perovskites Enables Broadening of Absorption Spectrum in Solar Cells. *J. Am. Chem. Soc.* **136,** 8094−8099 (2014).

49. Umari, P., Mosconi, E. & Angelis, F. De. Relativistic GW calculations on Perovskites for Solar Cell Applications. *Sci. Rep.* **9,** 1–7 (2014).

50. Bruno, A. & Chen, S. Lead-Free MA2CuClxBr4-x Hybrid Perovskites. *Inorg. Chem.* (2016). doi:10.1021/acs.inorgchem.5b01896

51. Giles E. Eperon, Tomas Leijtens, Kevin A. Bush, Rohit Prasanna, Thomas Green, Jacob Tse-Wei Wang, David P. McMeekin, George Volonakis, Rebecca L. Milot, Richard May, Axel Palmstrom, Daniel J. Slotcavage, Rebecca A. Belisle, Jay B. Patel, Elizabeth S. Parr, H. J. S. Perovskite-perovskite tandem photovoltaics with optimized bandgaps. *Science (80-.).* **354,**

861–865 (2016).

52. Innocenzo, V. D. *et al.* Tuning the Light Emission Properties by Bandgap Engineering in Hybrid Lead Halide Perovskite. *J. Am. Chem. Soc.* **136,** 17730−17733 (2014).

53. Grancini, G. *et al.* The Impact of the Crystallization Processes on the Structural and Optical Properties of Hybrid Perovskite Films for Photovoltaics. *J. Phys. Chem. Lett.* **5,** 3836−3842 (2014).

54. Borriello, I., Cantele, G. & Ninno, D. Ab initio investigation of hybrid organic-inorganic perovskites based on tin halides. *Phys. Rev. B - Condens. Matter Mater. Phys.* **77,** 1–9 (2008).

55. Filip, M. R., Eperon, G. E., Snaith, H. J. & Giustino, F. Steric engineering of metal-halide perovskites with tunable optical bandgaps. *Nat. Commun.* **5,** 1–9 (2014).

56. Quarti, C. *et al.* Environmental Science Structural and optical properties of methylammonium lead iodide across the tetragonal to cubic phase transition : implications for perovskite solar cells †. *Energy Environ. Sci.* **9,** 155–163 (2016).

57. Eperon, G. E. *et al.* Environmental Science Formamidinium lead trihalide : a broadly tunable perovskite for e ffi cient planar heterojunction solar. *Energy Environ. Sci.* **7,** 982–988 (2014).

58. Koh, T. M. *et al.* Formamidinium-Containing Metal-Halide: An Alternative Material for Near-IR Absorption Perovskite Solar Cells. *J. Phys. Chem. C* **118,** 16458−16462 (2014).

59. Pang, S. *et al.* NH2CH=NH2PbI3: An Alternative Organolead Iodide Perovskite Sensitizer for Mesoscopic Solar Cells. *Chem. Mater.* **26,** 1485−1491 (2014).

60. Nh, H. C., Lee, J., Seol, D., Cho, A. & Park, N. High-Effi ciency Perovskite Solar Cells Based on the Black. *Adv. Mater.* **26,** 4991–4998 (2014).

61. Yang, Noh, Jeon, K. High-performance photovoltaic perovskitelayers fabricatedthrough intramolecular exchange. *Science (80-.).* **348,** 1234–1237 (2015).

62. Giorgi, G., Fujisawa, J., Segawa, H. & Yamashita, K. Organic − Inorganic Hybrid Lead Iodide Perovskite Featuring Zero Dipole Moment Guanidinium Cations: A Theoretical Analysis. *J. Phys. Chem.* **119,** 4694−4701 (2015).

63. Marco, N. De *et al.* Guanidinium : A Route to Enhanced Carrier Lifetime and Open-Circuit Voltage in Hybrid Perovskite Solar Cells. *Nano Lett.* **16,** 1009−1016 (2016).

64. Pellet, N. *et al.* Mixed-Organic-Cation Perovskite Photovoltaics for Enhanced Solar- Light Harvesting ** Angewandte. *Angew. Chem. Int. Ed.* **53,** 3151–3157 (2014).

65. Mei, A. *et al.* A hole-conductor – free, fully printable mesoscopic perovskite solar cell with high stability. *Science (80-.).* **345,** (2014).

66. Mercier, N. (HO2C(CH2)3NH3)2(CH3NH3)Pb2I7: a predicted noncentrosymmetrical structure built up from carboxylic acid supramolecular synthons and bilayer perovskite sheets. *CrystEngComm* **2,** 429–432 (2005).

67. Choi, H. *et al.* Cesium-doped methylammonium lead iodide perovskite light absorber for hybrid solar cells. *Nano Energy* **7,** 80–85 (2014).

68. Michael Saliba,‡*ab Taisuke Matsui,‡c Ji-Youn Seo, a Konrad Domanski, a Juan-Pablo Correa-Baena, d Mohammad Khaja Nazeeruddin, b Shaik M. Zakeeruddin, a Wolfgang Tress, a Antonio Abate, a A. H. and M. G. Cesium-containing triple cation perovskite solar

cells: improved stability, reproducibility and high efficiency. *Energy Environ. Sci.* **9,** 1989–1997 (2016).

69. Kulbak, M., Cahen, D. & Hodes, G. How Important Is the Organic Part of Lead Halide Perovskite. *J. Phys. Chem. Lett.* **6,** 2452−2456 (2015).

70. Choi, H. *et al.* Cesium-doped methylammonium lead iodide perovskite light absorber for hybrid solar cells. *Nano Energy* **7,** 80–85 (2014).

71. Yuxi Tian Ivan G. Scheblykin. Artifacts in Absorption Measurements of Organometal Halide Perovskite Materials: What Are the Real Spectra? *J. Phys. Chem. Lett.* **6,** 3466−3470 (2015).

Appendix

The comparison of results taken from different studies highlighted many discrepancies. Indeed, it was noted that the value of the bandgap of a perovskite with the same components was calculated to be different depending on the study. For instance, the bandgap of the most studied perovskite $MAPbI_3$ was measured 1.504 eV[40], 1.51 eV[31,47], 1.52 eV[70], 1.55 eV[48], 1.575 eV[64], 1.58 eV[33],1.61 eV[56] and 1.70 eV[32]. The same occurred for $FAPbI_3$, whose bandgap was measured 1.47 eV[58], 1.48 eV[45,43] and 1.530 eV[64].

One of the reasons for these discrepancies might be the different way in which they extrapolated the bandgap from optical measurements. Indeed, some authors did it directly from the band edge of the absorption spectrum, while others did it by plotting the Tauc plot using the optical data. The Tauc plot shows the correlation between the absorption coefficient and the energy. For direct bandgap semiconductors, it was demonstrated that the absorption coefficient changes with the square route of the energy, while for indirect bandgap semiconductors, with the square of the energy. Since it has not yet been clearly demonstrated whether perovskites are direct or indirect semiconductors, there can be discrepancies between different studies even when they both used Tauc plots, depending on the assumptions they made for the bandgap nature of the perovskite.

A 2015 work[71] investigated the bandgap discrepancies and tried to give an answer to the question "What are the real spectra?". They found three different factors influence the shape of a perovskite absorption spectrum, namely the poor surface coverage of the sample, the high optical density of individual crystals and the light scattering. They assumed the absorption measured is equal to:

$$A_{measured} = -\log[\beta(1-\gamma(\lambda))10^{-OD(\lambda)} + (1-\beta)]$$

where OD is the optical density of individual crystals, β is the substrate coverage ratio, namely the are covered by the perovskite over the total area and $\gamma(\lambda)$ is the scattering coefficient, which is equal to 0 for no scattering and to 1 when all the coming light is scattered.

They observed that the scattering effect does not have an influence in the value of the bandgap. On the contrary, the presence of individual crystals does. In order to observe what was the effect of the single crystals size on $A_{measured}$, they set $\beta = 0.5$, no scattering, and changed the $OD(\lambda)$ by multiplying the experimental value of the OD of a single crystal by a factor ζ. Figure 21 shows the shift of the observed bandgap by increasing the thickness of the single crystals from $\zeta = 0.5$ to $\zeta = 8$ (when the thickness was estimated to be 1.2 μm).

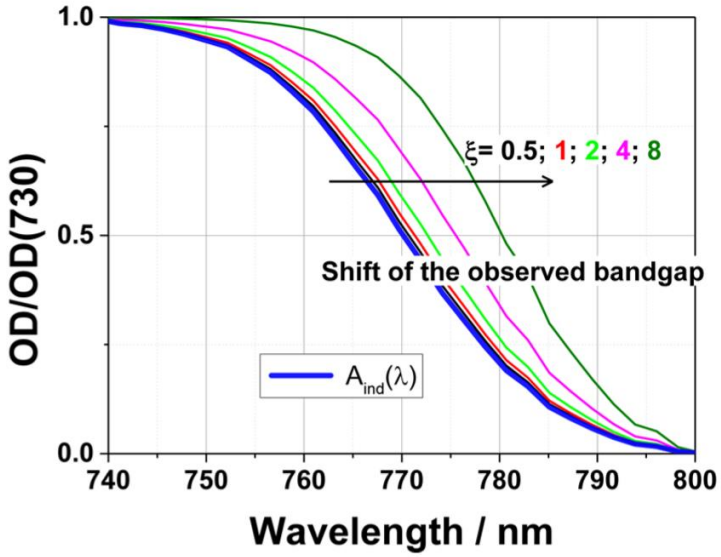

Figure 21: Effect of high optical density of single crystals on absorption edge position[71].

From this plot, however, it is not possible to observe the shift of the bandgap that they claim there is. Indeed, it appears that the onset of all the spectra are at 800nm, namely around 1.55 eV. In order to verify if their observation was correct, the Tauc plots for direct and indirect bandgap were drawn for the cases $\zeta = 1$ and $\zeta = 4$ (Figure 22 and 23).

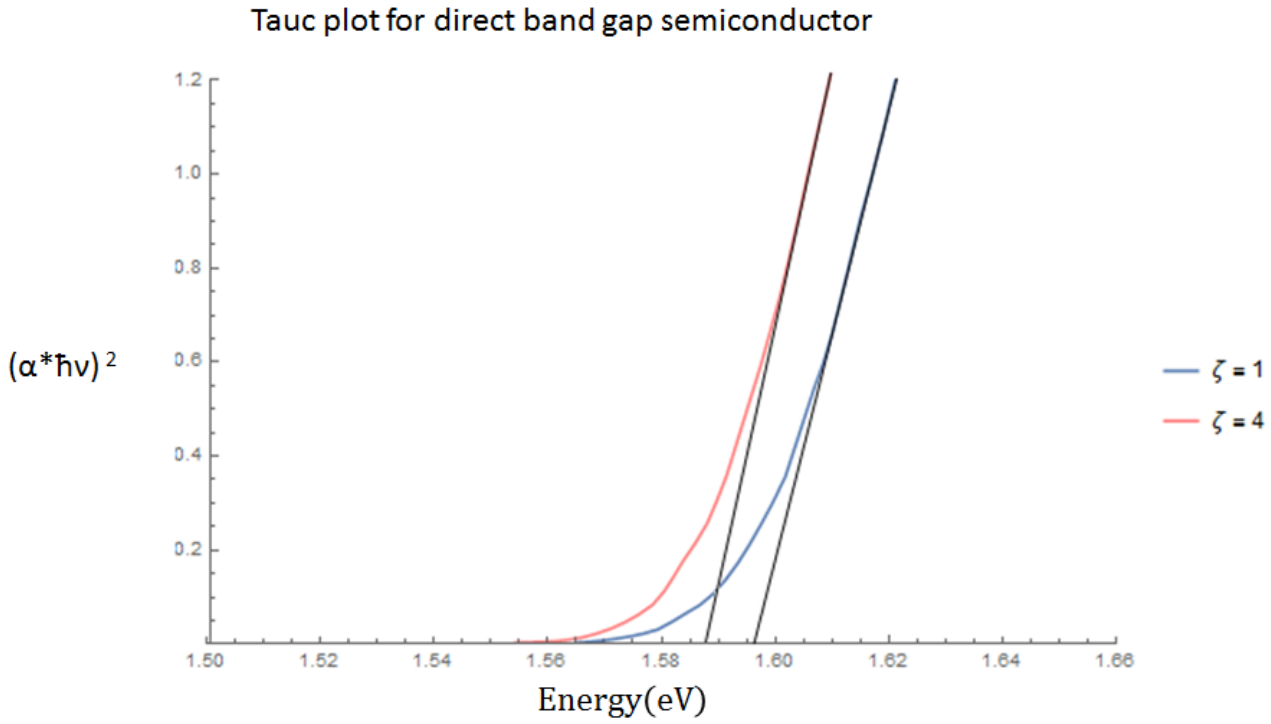

Figure 22: Tauc plot for direct bandgap semiconductor plotted from data extracted from figure 23 when ζ = 1 and 4.

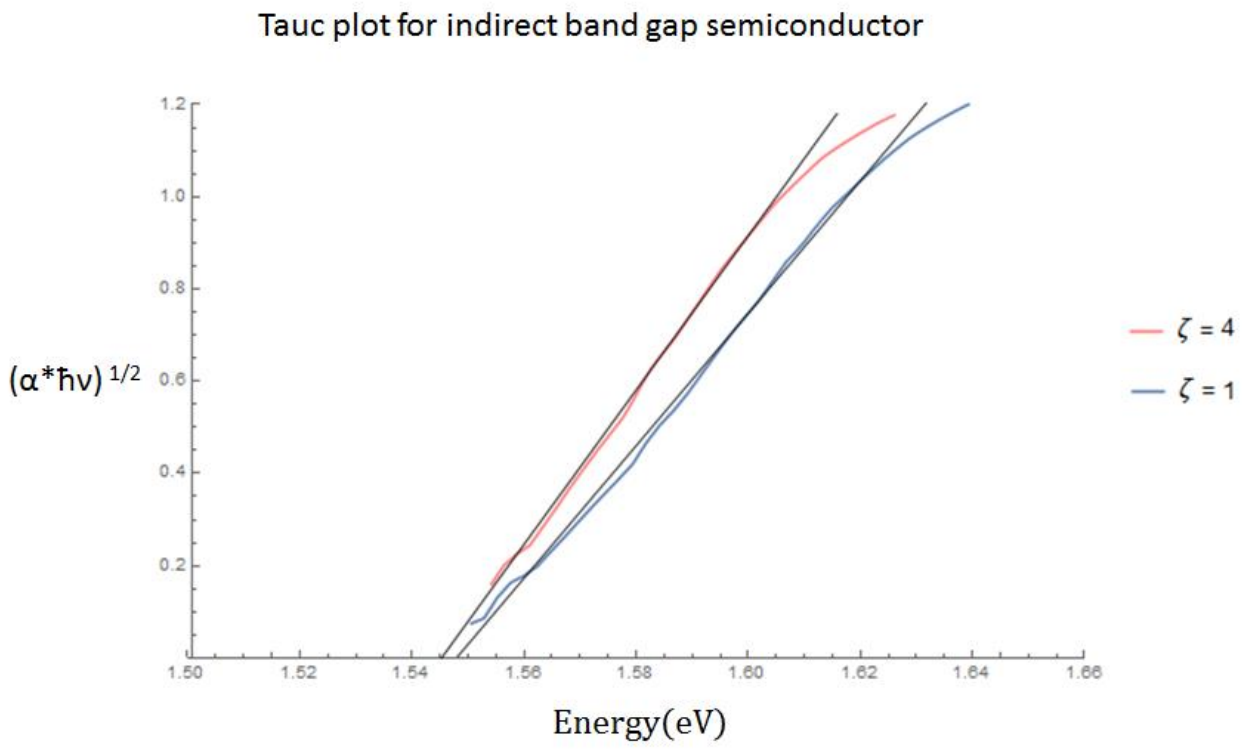

Figure 23: Tauc plot for indirect bandgap semiconductor plotted from data extracted from figure 23 when ζ = 1 and 4.

The plots show that there is indeed a shift in the bandgap value. Moreover, they display that the value of the bandgap is slightly different depending on how it is extrapolated, around 1.59 eV for direct bandgap assumptions and 1.55 eV for indirect bandgap assumptions. A final remark is that depending on the point of the curve in which the tangent was considered, the value of the bandgap shifts and this is moderately important for the direct bandgap case.

Even though these results seem to confirm the idea that the bandgap discrepancies depend on the inhomogeneity of the sample, other differences in the samples might generate a different value of the bandgap. Indeed, other studies[52] demonstrated that the optical absorption edge shifts to longer wavelengths when increasing the average crystallite dimension from less than 250 nm to more than 2 μm. They correlated this shift of the optical absorption edge with a bandgap shift without explicitly extrapolating the bandgap values from Tauc plots. To deposit nanocrystals, the perovskite solution was deposited on a Al_2O_3 mesoporous scaffold, while for bigger crystals a flat substrate was used. To explain the reason why the size of the crystals has an influence on the electronic properties of the perovskite, another study[53] carried out Raman spectroscopy analysis and optical analysis on samples with different crystal size and prepared with and without the addition of chloride, which plays a role in the crystallization process[10]. They found out that in flat films there is a reduced strain on the Pb-I cage than that present in mesoporous structure and that this is due to a different arrangement of the organic cations within inorganic cage. When the B and the X ions are not collinear, as explained in the A cation chapter, the energy of the CBM increases and the overall result is the bandgap broadening. Figure 24 shows the absorption edge trend when increasing the average crystallite size.

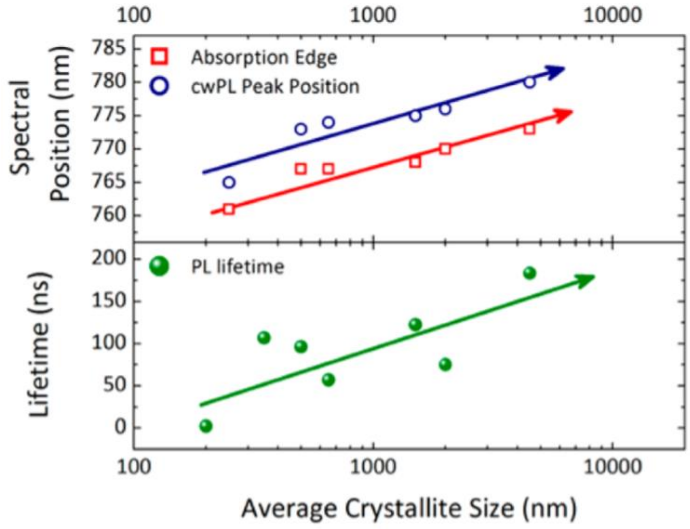

Figure 24: $MaPbI_3$ Absorption edge shift with average crystallite size (nm)[52].

Moreover, they found out that the presence of Cl^- in the crystallization process induces a preferred crystalline orientation so that the disorder in the mesoporous structure is reduced and the overall effect on the bandgap is weaker[53].

Overall, depending on the size of the crystals and on the surface coverage of the film, slightly different results may be obtained for the value of the perovskite bandgap. This could have a relevant effect in studies that try to predict the theoretical limit for the efficiency of perovskite solar cells, while it does not have a large relevance in this analysis because the differences in the values are very small compared to the differences in the bandgap values of perovskites composed of different elements or molecules.